IRN Hydrobio 4th workshop

2-5 Jun 2025
Orsay
France

Table of contents

Flow homogenization in adaptive microfluidic networks

Julien Bouvard*[1], Swarnavo Basu*[2], Charlott Leu[3], Onurcan Bektas[2], Joachim Rädler[3], Karen Alim[§2], and Gabriel Amselem[§1]

[1] *Laboratoire d'Hydrodynamique (LadHyX), CNRS, Ecole Polytechnique, Institut Polytechnique de Paris, 91120 Palaiseau, France*

[2] *Center for Protein Assemblies and Department of Bioscience, School of Natural Sciences, Technische Universität München, 85748 Garching, Germany*

[3] *Faculty of Physics and Center for NanoScience, Ludwig-Maximilians-Universität München, 80539 Munich, Germany*

From the vasculature of animals to the porous media making up batteries, the core task of flow networks is to transport solutes and perfuse all cells or media equally with resources. Yet, living flow networks have a key advantage over porous media: they are adaptive and self-organize their geometry for homogeneous perfusion throughout the network. Here, we show that artificial flow networks with an initial random geometry and inhomogeneous perfusion profile can be re-organized towards more homogeneous perfusion by flowing through them a reactive chemical that erodes the network walls. Flowing a pulse of cleaving enzyme through a network patterned into an erodible hydrogel, with initial channels disparate in width, we observe a homogenization in channel resistances. Experimental observations are matched with numerical simulations of the diffusion-advection-sorption dynamics of an eroding enzyme within a network. Analyzing transport dynamics theoretically, we show that homogenization only occurs if the pulse of the eroding enzyme lasts longer than the time it takes any channel to equilibrate to the pulse concentration. The equilibration time scale derived analytically is in agreement with simulations. Last, we show both numerically and experimentally that erosion leads to the homogenization of complex networks containing loops. Erosion being an omnipresent reaction, our results pave the way for a very versatile self-organized increase in the performance of porous media.

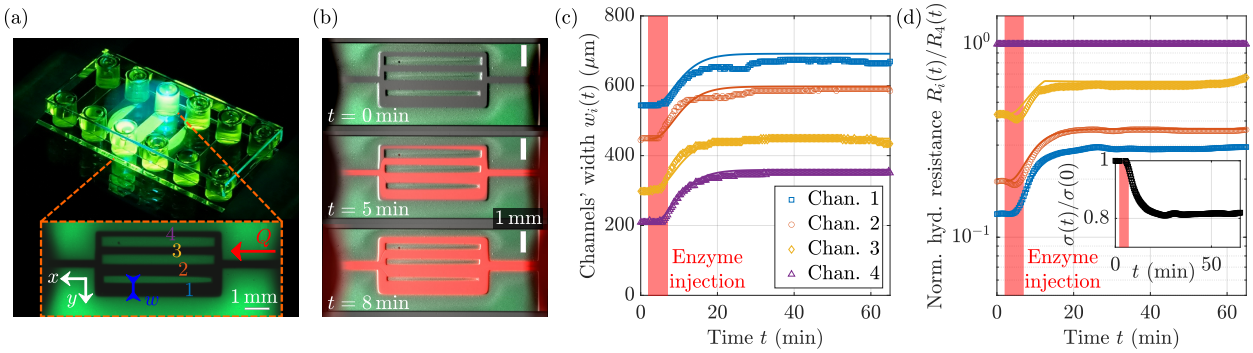

FIG. 1. (a) Typical experimental setup: A network of 4 parallel channels (black) is prepared, with walls made of an erodible hydrogel (green). (b) Timelapse of a pulse of eroding enzyme (red) being flowed through the network. Scale bar: 1 mm. (c) All channel widths increase as a result of enzyme injection. (d) The hydrodynamic resistances of all channels evolve as a result of erosion, and homogenize, leading to more homogeneous perfusion. Inset: standard deviation of the channel resistances as a function of time.

From Stokes to Maxwell: an electrostatic perspective on viscous Marangoni flows

Thomas Bickel[1] and François Detcheverry[2]

[1] *LOMA, University of Bordeaux, F-33400 Talence, France,* thomas.bickel@u-bordeaux.fr
[2] *ILM, University of Lyon, F-69622 Villeurbanne, France,* francois.detcheverry@univ-lyon1.fr

When a drop of dishwashing liquid is deposited on the surface of water previously sprinkled with pepper, one observes a rapid outward flow that drives the peppercorns towards the edges of the bowl. This simple yet captivating kitchen experiment is a classic demonstration of the Marangoni effect − fluid motion driven by surface tension gradients. Beyond this everyday observation, the Marangoni effect plays a crucial role in a wide range of phenomena, from stabilizing soap films to enabling the self-propulsion of active particles at the water-air interface.

From a theoretical viewpoint, Marangoni flows are governed by the Navier-Stokes equation, which describes fluid motion, and the advection-diffusion equation, which characterizes the transport of surfactants. The problem happens to be highly nonlinear due to the dominance of advection over diffusion, making analytical progress particularly challenging. In this talk, I will show that Marangoni flow in a deep liquid layer and in the viscous regime (Re=0) can be mapped onto an electrostatic problem. This mathematical equivalence provides a simple way to establish novel analytical solutions to the spreading dynamics. More intriguingly, the electrostatic analogy can be extended further down the molecular scale. Indeed, surfactant spreading can be formally described as a set of N particles interacting via an effective Coulomb potential. The spreading dynamics then emerges from Newton's equations of motions, entirely bypassing hydrodynamic considerations. This unconventional analogy therefore offers a fresh and effective perspective on Marangoni flows.

Orbiting droplets on a soap film: toward gravitational analogues

Jean-Paul Martischang[1], Benjamin Reichert[1], Germain Rousseaux[2], Alexis Duchesne[1], and Michael Baudoin[1,*]

[1] *Univ. Lille, CNRS, Centrale Lille, Univ. Polytechnique Hauts-de-France, UMR 8520, IEMN, F59000 Lille, France,* michael.baudoin@univ-lille.fr

[2] *Institut Prime (UPR 3346), CNRS - Université de Poitiers - ISAE ENSMA, 11 Boulevard Marie et Pierre Curie Téléport 2 - BP 30179, 86962 Futuroscope Chasseneuil Cedex, France*

ABSTRACT

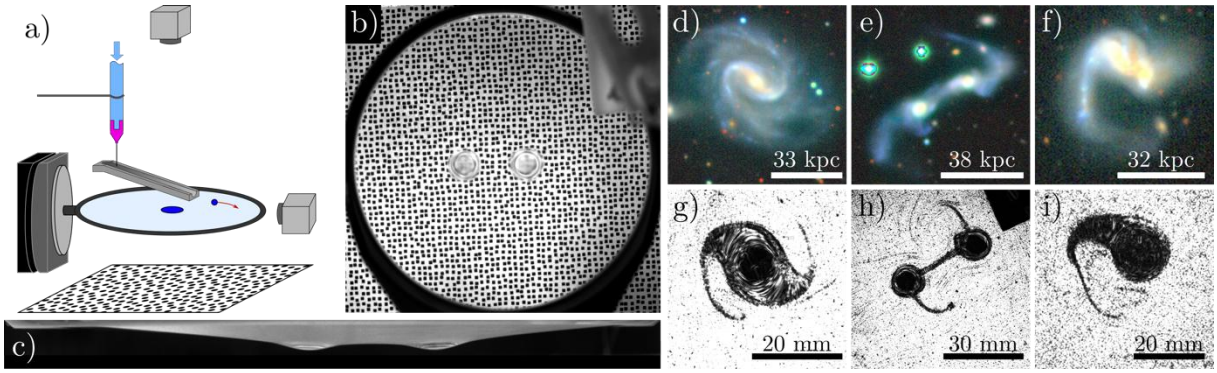

FIG. 1. Droplets orbiting and merging on a soap film and resulting structures. (a) Sketch of the experimental setup. (b) and (c) Images of two orbiting drops on a soap film from above and from aside respectively. (d-f) Images of structures resulting from the interactions of two orbiting drops and comparison to similar galaxy structures (g-i)

In this work [1], we present experimental observations and theoretical modeling of droplets orbiting, interacting, and merging on a horizontal soap film. We first demonstrate that a droplet deposited at the center of the film induces a deformation governed by a balance between gravitational and capillary forces, resulting in a stable lens-shaped structure with a universal radius, independent of the droplet's mass. We then show that when a droplet is placed off-center, the resulting deformation generates a restoring force directed toward the center, creating a harmonic potential well that causes the droplet to oscillate around the film's center. Introducing a second droplet with a non-zero initial velocity leads to sustained orbital dynamics and, eventually, to complex merging scenarios characterized by spiral arm formations and tidal-like deformations—features reminiscent of galaxy mergers in astrophysics. These behaviors arise from a pairwise attractive force mediated by the gravito-capillary deformation of the film, effectively mimicking a two-dimensional analogue of Newtonian gravity. This work establishes a versatile laboratory platform to explore gravitational analogues at human scales, offering novel insights into the dynamics of systems typically observed only at astronomical scales.

[1] J.P. Martischang, B. Reichert, G. Rousseaux, A. Duchesne, and M. Baudoin, Orbiting, colliding and merging droplets on a soap film: toward gravitational analogues, submitted arXiv:2503.08331 (2025)

Electrospray of a leaky dielectric liquid

[1]Abhiram Hens, [2]Gautam Biswas*

[1]Department of Chemical Engineering, National Institute of Technology, Durgapur West Bengal, India, 713209

[2]Department of Mechanical Engineering, Birla Institute of Technology & Science, Pilani, K.K. Birla Goa Campus, India, 403726

ABSTRACT

In this investigation, a detailed computational study, using two-dimensional axisymmetric frame work, on the nonlinear behaviors of electrohydrodynamic flows of a leaky dielectric liquid emanating from a nozzle in the form of a spray, is conducted. A leaky dielectric fluid has low but non-zero conductivity. Taylor pioneered a model related to leaky dielectric fluids where it was assumed that the bulk fluid medium is free of charges and charge accumulation occurs only at the interface [1,2]. The drops of a dielectric fluid get deformed in the presence of a steady electric field [3–5]. Such a phenomenon has a significant influence on the electrosprays. Electrosprays find several applications in the areas of material coating, agricultural sprays, drug delivery, and mass spectrometry. The entire set of coupled equations, including the Navier-Stokes equations, simplified Maxwell's equations, and constitutive equations, is solved using an in-house code based on Coupled Level Set and Volume of Fluid (CLSVOF) method [6]. The dynamics of the dispersed flow of a leaky dielectric liquid emanating from the orifice of a nozzle (needle) depends on several parameters, such as the flow rate, electric field intensity, surface tension, Coulombic forces, electrophoretic forces. etc. Different jetting regimes, such as choked jets, pulsating jets, steady cone jets, and multi jets, were observed based on these conditions. Variation of the drop diameters and jet break-up length at different flow rates were studied and the results were compared with the available experimental results. The results provide deeper understanding of the mechanisms that govern jet stability, breakup, and drop formation.

References

[1] G. I. Taylor, Disintegration of water drops in an electric field, ***Proc R Soc London, Ser A***, 280 (382) 383–397 (1964).

[2] D.A. Saville, Electrohydrodynamics: The Taylor-Melcher Leaky Dielectric Model, ***Annu. Rev. Fluid Mech***. 29 (1), 27–64 (1997).

[3] M.P. Borthakur, G. Biswas, D. Bandyopadhyay, Dynamics of drop formation from submerged orifices under the influence of electric field, ***Physics of Fluids,*** 30 (12), 122104 (2018).

[4] Z. Wang, Q. Wang, B. Li, Y. Zhang, J. Wang, J. Tu, An experimental investigation on cone-jet mode in electrohydrodynamic (EHD) atomization, ***Exp. Therm. Fluid Sci.,*** 114, 110054 (2020).

[5] R.T. Collins, J.J. Jones, M.T. Harris, O.A. Basaran, Electrohydrodynamic tip streaming and emission of charged drops from liquid cones, ***Nat. Phys.***, 4(2), 149–154 (2008).

[6] D. Gerlach, G. Tomar, G. Biswas, F. Durst, Comparison of volume-of-fluid methods for surface tension-dominant two-phase flows, ***International Journal of Heat Mass Transfer,*** 49 (3-4), 740-754, (2006).

*Email: gtm@iitk.ac.in, gautamb@goa.bits-pilani.ac.in

Looking for Singularities in Turbulence

B. Dubrulle[1]

[1] *CNRS, SPEC, University Paris-Saclay, France,* berengere.dubrulle@cea.fr

Turbulence, a phenomenon observed by physicists in natural and laboratory flows, is thought to be described by Navier-Stokes equations (NSE). Mathematicians are wondering whether NSE are well posed, namely whether they can develop a singularity in finite time from regular initial conditions. Given that, it is natural to investigate regularity properties of turbulence.
In this talk, I will review available tools to investigate statistical and deterministic regularity of turbulent flows, some of which are directly inspired from regularity tools developed by mathematicians for NSE. I will also describe the results of application of such tools to numerical simulations of NSE or to state-of-the art experimental measurements and discuss their link and potential implication regarding regularity properties of NSE.

Surface and internal waves in a shear flow

Anil Kumar[1], S. Ravichandran[2] and Ratul Dasgupta[1]

[1] *Department of Chemical Engg., IIT Bombay, Powai, Mumbai 400 076*
[2] *Climate Studies, IIT Bombay, Powai, Mumbai 400 076*

We study a classical model[1, 2] of hydrodynamic instability in an inviscid shear flow containing a sharp density interface in a stably stratified configuration (i.e. light over heavier fluid). The base-state velocity in the less dense fluid increases exponentially with increasing vertical distance, asymptotically reaching a constant value, see left panel below. The lighter fluid is quiescent in the base-state. Since the series of studies by Miles[3, 4, 5] it has been known that unlike homogenous flows, such non-inflectional velocity profiles with a sharp density interface can be *inviscidly* unstable. The instability mathematically owes its origin to the presence of a logarithmic singularity (the so-called critical layer)[6] in the solution to the Rayleigh equation when the base-state velocity profile has convex curvature at this location. The multi-valuedness resulting from this logarithmic singularity, generates a phase shift between the perturbation pressure just above the density interface and the density interface itself. Due to this, a mechanism of extracting energy from the base-state becomes possible thereby generating instability and as a consequence, waves at the density interface. This `Miles' mechanism of instability on has been extensively studied in the context of wind generation of water waves since the first suggestion of this by Jeffreys[7].

For this aforementioned exponential model, the Rayleigh equation can be analytically solved in terms of the Gauss hypergeometric function yielding the dispersion relation and eigenfunctions in closed analytical form[8]. We study this instability analytically and numerically in the non-dimensional space of Froude number, Bond number and density ratio. It is shown that the nature of instability undergoes a qualitative change as non-dimensional parameters are varied (see right panel below). We show that for the fastest growing Fourier mode, the Reynolds shear stress associated with the perturbation velocities transitions from a Heaviside function like shape with a near discontinuous jump at the critical layer (see right panel below) to a smooth curve whose peak value appears at the density interface instead of the critical layer location, as density ratio is varied. We argue that this change indicates a cross over from the Miles mechanism to another distinct mechanism of instability of the Kelvin-Helmholtz kind, the critical layer playing a dominant role in the former but a sub-dominant role in the latter case. Several other metrics are also used to support our conclusions viz. the vertical variation of the perturbation kinetic energy, the phase difference between the perturbation pressure above the density interface and the interface itself etc.. Linearised analytical predictions receive strong support from nonlinear simulations of the incompressible Euler's equations with gravity and surface tension. These simulations also reveal several interesting and novel features in the nonlinear regime[9].

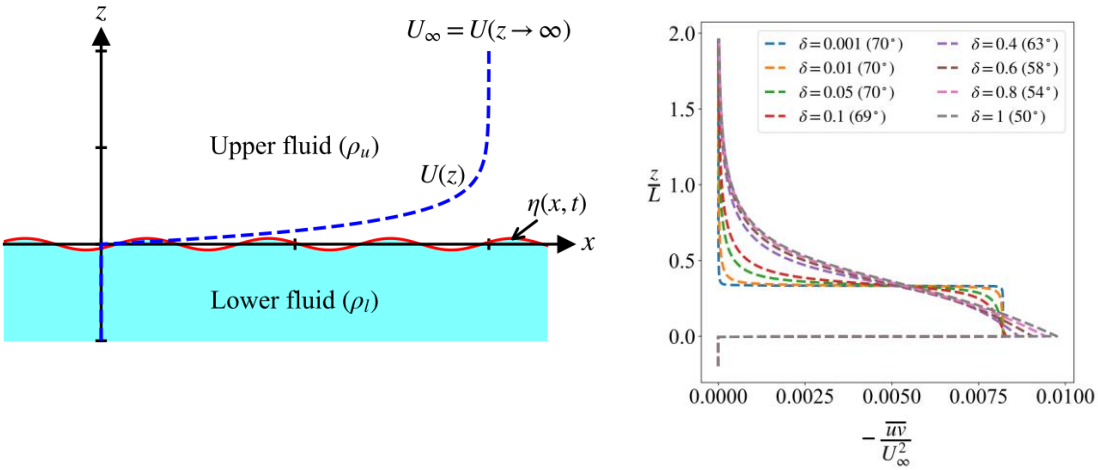

(Left panel) Base-state velocity profile (Right panel) Reynolds stress as a function of vertical distance at various density ratio. As the density ratio is varied, note the change in shape of the Reynolds stress for the fastest growing mode.

References:

[1] Hughes, T. H., and W. H. Reid. "On the stability of the asymptotic suction boundary-layer profile." *Journal of Fluid Mechanics* 23.4 (1965): 715-735.

[2] Morland, L. C., and P. G. Saffman. "Effect of wind profile on the instability of wind blowing over water." *Journal of Fluid Mechanics* 252 (1993): 383-398.
[3] Miles, John W. "On the generation of surface waves by shear flows." *Journal of Fluid Mechanics* 3.2 (1957): 185-204.
[4] Miles, John W. "On the generation of surface waves by shear flows. Part 2." *Journal of Fluid Mechanics* 6.4 (1959): 568-582.
[5] Miles, John W. "On the generation of surface waves by shear flows Part 3. Kelvin-Helmholtz instability." *Journal of Fluid Mechanics* 6.4 (1959): 583-598.
[6] Tollmien, Walter 1930 Über die entstehung der turbulenz. Vorträge aus dem Gebiete der Aerodynamik und verwandter Gebiete: Aachen 1929 pp. 18–21.
[7] Jeffreys, H. 1925 On the formation of water waves by wind. Proc. R. Soc. Lond. A 107 (742), 189–206.
[8] Young, W.R. & Wolfe, C.L. 2014 Generation of surface waves by shear-flow instability. J. Fluid Mech. 739, 276–307.
[9] Surface and internal waves in a shear flow – transition from the Miles instability, Anil Kumar, S. Ravichandran and Ratul Dasgupta, 2025 (To be submitted)

Hysteresis alters the flow near a moving contact line: evidence from experiments and simulations

Harish N Dixit[1], V. S. Anvesh Sangadi[2], Charul Gupta[2], Anjishnu Choudhury

[1] *Dept. of Mechanical & Aerospace Engg. & Centre for Interdisciplinary Programs, IIT Hyderabad, India,* hdixit@mae.iith.ac.in

[2] *Dept. of Mechanical & Aerospace Engg., IIT Hyderabad, India,* me20m22p100001@iith.ac.in

[2] *Dept. of Mechanical & Aerospace Engg., IIT Hyderabad, India,* me20m22p100001@iith.ac.in

[2] *Dept. of Mechanical & Aerospace Engg., IIT Hyderabad, India,* charul.gupta229@gmail.com

[2] *Dept. of Mechanical Engg., IIT Bombay, India,* a.choudhury@iitb.ac.in

ABSTRACT

A moving contact line is a region where the interface between two immiscible fluids intersects a moving solid surface. The theoretical study by Huh & Scriven [1] reported a stress singularity near a moving contact line. The stress singularity is primarily caused by the application of the no-slip boundary condition on the moving plate, which is directly in conflict with a moving contact line. Several models have been proposed to resolve this singularity. A popular choice is to relax the no-slip condition and allow a finite amount of slip in the vicinity of the moving contact line [2,3]. The first goal of the present is to provide evidence for slip flow near a moving contact line using high-resolution PIV experiments. The experiments reveal the presence of variable slip in the vicinity of the moving contact line and no slip further away, thus offering a direct pathway for the resolution of the moving contact line paradox. The second goal of the study is to examine the effect of dynamic hysteresis on the flow field. In the absence of hysteresis, the flow field in experiments is found to be in excellent agreement with theory. But higher values of hysteresis can have a dramatic effect on the flow field. Hysteresis induces a high-frequency fluctuation at the contact line due to the localised 'stick-slip' motion. The effect of this fluctuation is investigated in the present study using experiments and numerical simulations.

I. INTRODUCTION

Moving contact lines can be observed in several applications, such as ink-jet printing, coating, secondary oil recovery, etc. Huh & Scriven [1] studied the flow field near a moving contact line assuming the interface to be flat and the no-slip condition was employed on the moving solid. This leads to the formation of a stress singularity, sometimes referred to as the Huh & Scriven paradox. Several models [2, 3] have subsequently been developed to resolve the moving contact line singularity. A common theme in all these models is the incorporation of additional physics at the moving contact line such as intermolecular forces, phase-field models or slip near the contact line. It is well known that introducing slip near the moving contact line resolves the stress singularity and is one of the most popular choices for modelers. In a recent discovery [4,5], it was shown that slip flow indeed occurs in the vicinity of the moving contact line.

Another observation with moving contact lines is the presence of contact angle hysteresis. When the static contact angle varies between two different values, it is referred to as the static contact angle hysteresis. This value can easily be measured using a standard contact angle meter. Contact angle hysteresis also occurs in a dynamic scenario, but its value, defined as $\Delta\theta_d$ is difficult to measure in experiments. Several factors affect the value of $\Delta\theta_d$ such as roughness of the moving substrate, chemical heterogeneity on the substrate, and the nature of the fluids. In the present experiments, we find that glass substrates with silicone oils exhibit low values of static hysteresis, typically less that 5^o. But on the other hand, in the case of water and sugar-water mixtures on glass substrates, we find static hysteresis was

[1] Huh, C. & Scriven, L. E., Hydrodynamic model of steady movement of a solid/liquid/fluid contact line. J. Coll. Int. Sci., **35(1)**, 85-101 (1971)

[2] Cox RG., The dynamics of the spreading of liquids on a solid surface. Part 1. Viscous flow, J. Fluid Mech., 168, 169-194, (1986)

[3] Kirkinis E, Davis SH, Moffatt vortices induced by the motion of a contact line. J. Fluid Mech.,746:R3 (2014)

[4] Gupta, C., Chandrala, L.D. and Dixit, H.N., An experimental investigation of flow fields near a liquid–liquid moving contact line. The Euro. Phys. Journal Special Topics, pp.1-11. (2024)

[5] Gupta, C., Choudhury, A., Chandrala, L.D. and Dixit, H.N., An experimental study of flow near an advancing contact line: a rigorous test of theoretical models. Journal of Fluid Mechanics, 1000, pp. A45 (2024)

large, typically ranging from 40^o to 60^o. Such large differences between the two cases suggests that even the dynamic hysteresis differs by a large value between silicone oils and water-based fluids. Experimentally, we find a dramatic difference in the

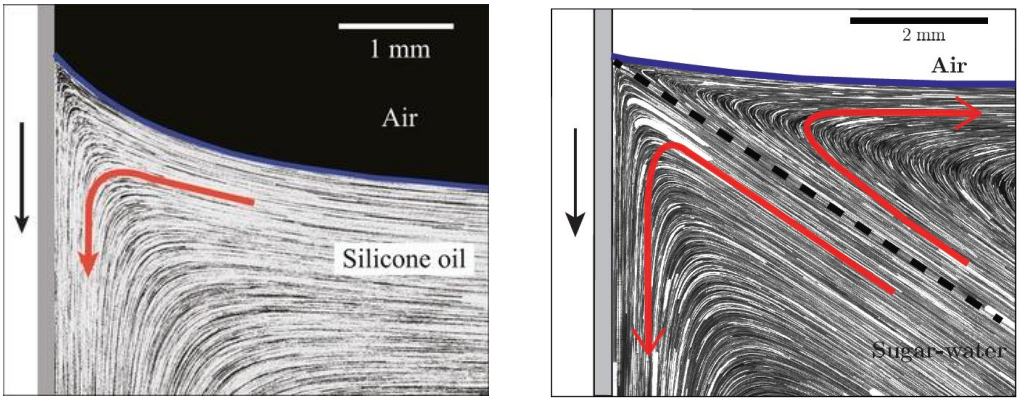

Fig. 1: Streakline flow showing rolling motion obtained for small hysteresis (left panel), split-streamline flow obtained with large hysteresis (right panel)

flow field as shown in figure 1. In the case of silicone oil, the flow field exhibits a rolling motion consisting with the theoretical predictions of Huh & Scriven's theory, whereas with sugar-water mixtures, the flow exhibits split-streamline motion. To confirm this, we conduct numerical simulations using *Basilisk* by imposing a fluctuating contact angle boundary condition. The results of the simulations are shown in figure 2. Application of hysteresis in the simulations changes the flow from a rolling type to a split-streamline type consistent with experimental observations.

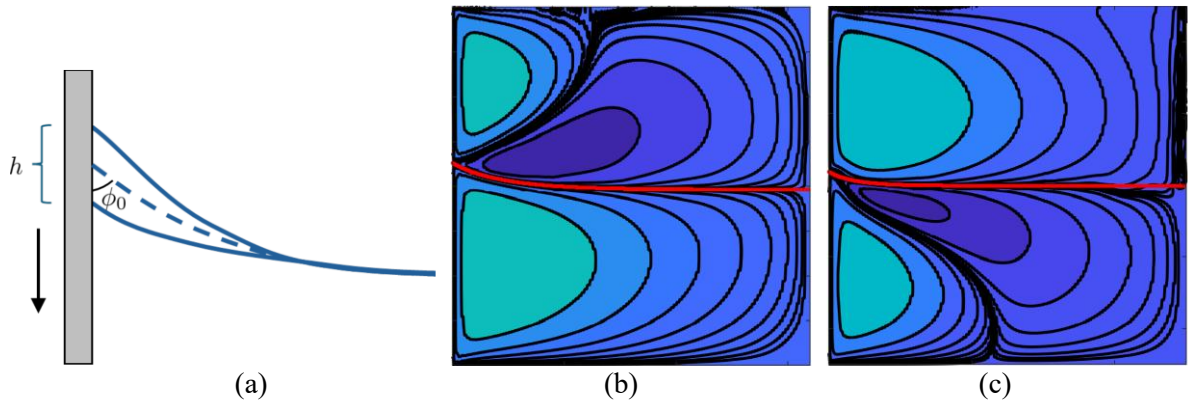

Fig. 2: (a) Boundary condition at the moving contact line, (b) streamfunction contours with no hysteresis exhibits rolling motion in the lower fluid, (c) streamfunction contours with hysteresis exhibits split-streamline motion.

This shows that the change in the flow of the field observed in experiments can indeed be explained in terms of dynamic hysteresis, and to the best of our knowledge, this is the first such observation in the literature.

ACKNOWLEDGEMENTS

HND gratefully acknowledges funding from the Science & Engineering Research Board, Department of Science and Technology for financial support through grant CRG/2021/007096.

Wetting properties of water on ice

Christophe Josserand

[1]*Laboratoire d'Hydrodynamique, LadHyX, UMR7646 CNRS & Ecole Polytechnique, IPParis, Palaiseau, France*
Christophe.josserand@polytechnique.edu

Wettability quantifies the affinity of a liquid over a substrate, and determines whether the surface is repellent or not. When both the liquid and the solid phases are made of the same chemical substance and are at thermal equilibrium, complete wetting is expected in principle, as observed for instance with drops of molten metals spreading on their solid counterparts. However, this is not the case for water on ice. Although there is a growing consensus on the partial wetting of water on ice and several estimates available for the value of the associated contact angle, the question of whether these values correspond to the equilibrium angle or not is still open. In the talk, we will address this issue experimentally and demonstrate the existence of a small, non-vanishing equilibrium contact angle of water on ice whose value is close to 12°. Indeed, when depositing water droplets on ice layers with accurately controlled surface temperatures, we evidence that droplet spreading is unaffected by thermal effects and phase change close enough to the melting point, where the liquid film relaxes to a stable sessile drop shape. Whereas the short time dynamics is driven by an inertial-capillary balance, the evolution towards equilibrium is described by a Cox-Voinov dynamics and is therefore capillary - and not thermally - related. This way, we show that the measured macroscopic contact angle at the end of the spreading process is indeed an equilibrium one, and that it remains constant for undercoolings below 1 K. This measurements is in agreement with those made on the meniscus formed when a ice layer is withdrawn from a water bath in a steady regime.

The experimental setup is schematized in figure 1-a. Experiments consist in depositing a pendent drop of pure demineralized water of density ρ, viscosity η and surface tension γ at vanishing impact velocity (using a linear stage) on a flat layer of ice made of the same pure demineralized water, whose surface temperature is T_i.

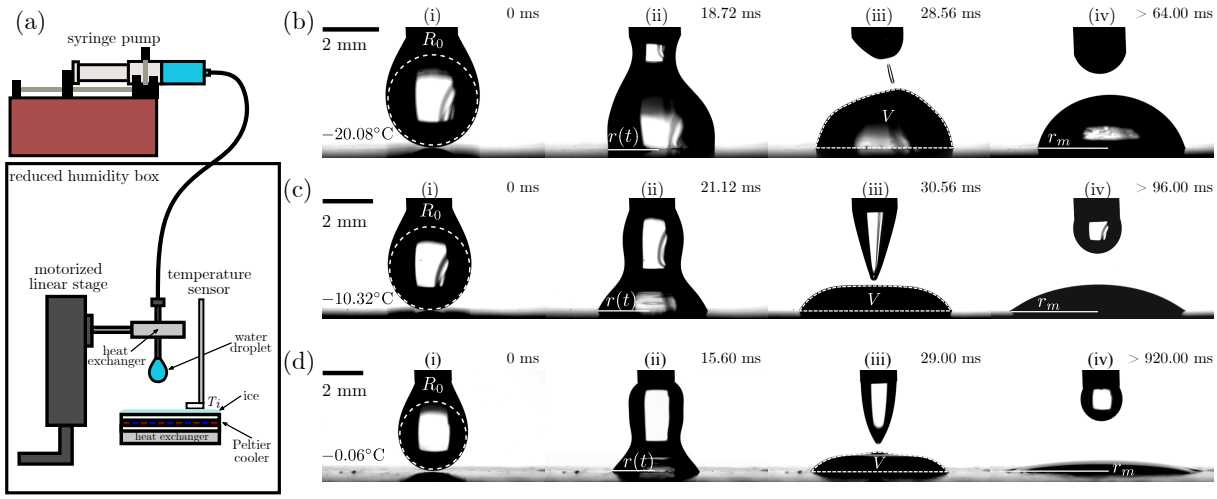

Typical spreading dynamics are shown on figure 1-b, showing that the spreading is higher when approaching the melting temperature, though it always stops, suggesting that the contact angle of water on ice is not zero. We will discuss these results in more details, demonstrating that the contact angle of water on ice at thermodynamical equilibrium is 12° (+/- 1°).

We anticipate this key finding to significantly improve the understanding of capillary flows in the presence of phase change, which is especially useful in the context of ice morphogenesis and of glaciology, but also in the aim of developing numerical methods for resolving triple-line dynamics.

Derivation and test of the constitutive law for the viscous stress tensor of incompressible two-phase flows of Newtonian fluids

Jacques Magnaudet[1], Hadrien Bruhier, Samuel Mer and Thomas Bonometti

[1] *IMFT, CNRS and University of Toulouse, Toulouse, France,* jacques.magnaudet@toulouse-inp.fr

We consider how the exact Navier-Stokes equations describing a two-phase flow at the local level are altered by the spatial filtering inherent to the discretization process. Combining an exact filtered solution valid in a specific 2D configuration with generic continuum mechanics results for the behavior of anisotropic fluids, we show that the proper form of the viscous stress tensor to be used in computations is anisotropic and involves two viscosity coefficients instead of one in a usual Newtonian fluid. Predictions of this model are then tested against original experimental data obtained in a viscous buoyancy-driven exchange flow generated by unstably superimposing two immiscible fluids with a large viscosity contrast in a closed vertical pipe. It is shown that, compared with usual ad hoc models for the viscous stress tensor, the anisotropic model is the only one capable of predicting correctly the flow evolution at a reasonable computational cost.

Hydrodynamics of microlayer in boiling

Corentin Le Houedec[1], Cassiano Tecchio[1], Linkai Wei[1], Guillaume Bois[1],
Pere Roca i Cabarrocas[2], Pavel Bulkin[2] and Vadim Nikolayev[3]
[1] *Laboratory of Thermohydraulics and Fluid Mechanics, CEA Paris-Saclay and Paris-Saclay University*
[2] *Laboratory of Physics of Interfaces and Thin Films, Ecole Polytechnique, Institut Polytechnique de Paris*
[3] *Laboratory of Condensed Matter Physics, CEA Paris-Saclay, CNRS and Paris-Saclay University, France,*
vadim.nikolayev@cea.fr

The microlayer is a μm-thick layer of liquid that commonly forms between the heater and growing on it vapor bubble in nucleate boiling. It is extremely important because of the large portion of heat transferred through it. Our recent studies [1] showed that its formation is analogous to the Landau-Levich film deposition. We describe here the experimental installation (Fig. 1) in which we generate a single bubble at a time on the indium-tin oxide (ITO) film. To heat the ITO, we use a permanent infra-red (IR) laser, the energy of which is absorbed by ITO but not by the MgF_2 substrate entirely transparent in the IR bandwidth. The bubble nucleation is controlled by the artificial geometrical defect, which is a ~20-50μm diameter hole fabricated at the MgF_2 surface prior to the ITO deposition. The IR laser is centered on the defect.

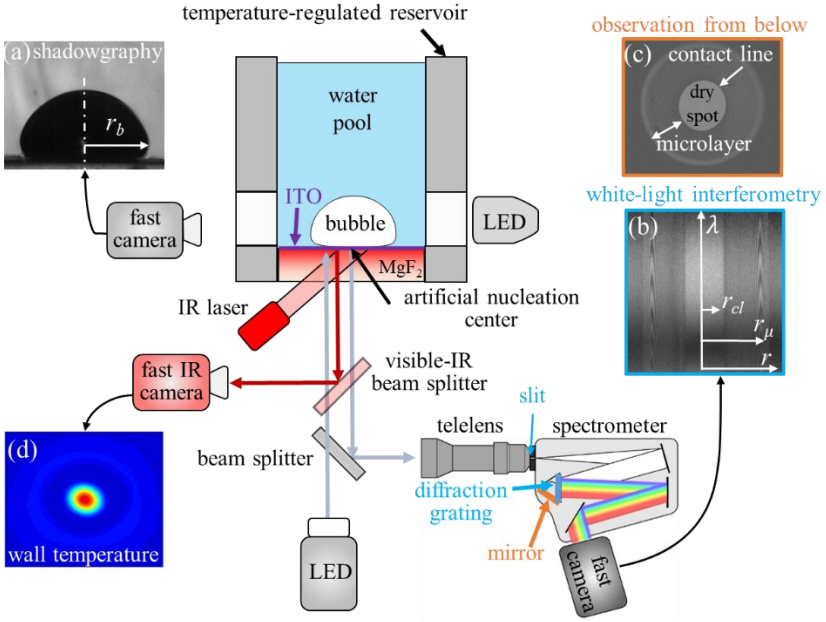

FIG. 1. Scheme of the experimental setup and the optical diagnostics: (a) side-wise bubble shadowgraphy; (b) white-light microlayer interferometry; (c) direct observation of dry spot and microlayer from below; (d) infra-red (IR) thermography.

Three synchronized fast and high-resolution cameras film at 4000 fps. They perform side-wise bubble shadowgraphy (Fig. 1a), infra-red thermography (IRT) (Fig. 1d) and white-light interferometry (Fig. 1b). The latter camera can be alternatively used for the direct observation from below (Fig. 1c) that serves for checking of the bubble axial symmetry and centering on the defect.

The bubble growth and departure cycles are periodical so only one of them is sufficient to study [2]. In the beginning, the bubble growth is so fast that the vapor-liquid solid contact line (of radius r_{cl}) recedes slower than the bubble edge (of the radius r_μ). This corresponds to $t \in [0, t_\mu^{max}]$ in Fig. 2.

[1] C. Tecchio, X. Zhang, B. Cariteau, G. Zalczer, P. Roca i Cabarrocas, P. Bulkin, J. Charliac, S. Vassant, V. S. Nikolayev, Microlayer in nucleate boiling seen as Landau-Levich film with dewetting and evaporation. *J. Fluid Mech.* **989**, A4 (2024).
[2] C. Tecchio, B. Cariteau, C. Le Houedec, G. Bois, E. Saikali, G. Zalczer, S. Vassant, P. Roca i Cabarrocas, P. Bulkin, J. Charliac & V. S. Nikolayev, Microlayer evaporation during bubble growth in nucleate boiling, *Int. J. Heat Mass Transf.* **231**, 125860 (2024).

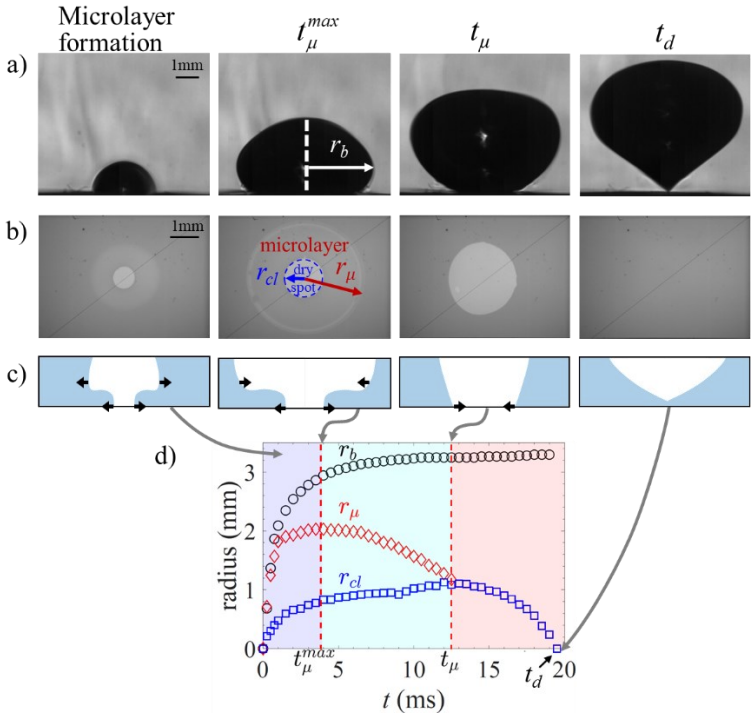

FIG. 2. Bubble growth stages shown with (a) experimental sidewise shadowgraphy images, (b) experimental bottom view images and (c) corresponding microlayer schematics. (d) The dynamics of the radii of bubble (r_b), microlayer (r_μ), and contact line (r_{cl}).

decrease. The advancing bubble edge meets the contact line at $t = t_\mu$ and microlayer disappears. The bubble finally departs at $t = t_d$. The microlayer shape measured with the white light interferometry shows a bumped shape that can be explained by using the Landau-Levich theory [1].

The microlayer dynamics can be modelled with the lubrication approximation [1] or with the direct numerical simulation (DNS) [3][4] by using the multiscale approach within the TRUST/TrioCFD freeware employing the front tracking numerical method to resolve the moving vapor-liquid interface (Fig. 3).

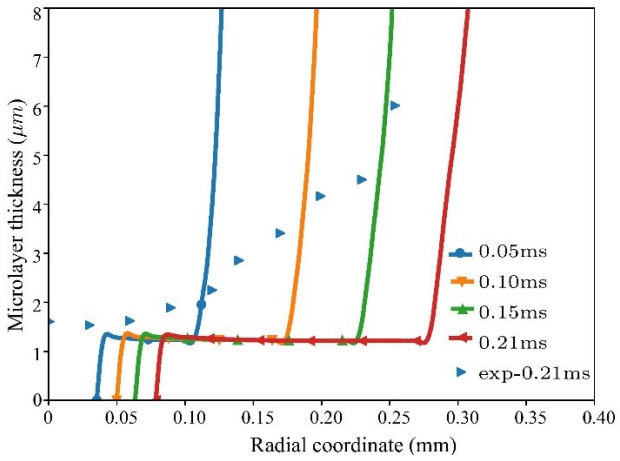

FIG. 3. DNS simulations of microlayer dynamics [4].

[3] L. Wei, G. Bois, V. Pandey & V. S. Nikolayev, Effect of contact line evaporation during nucleate boiling studied by multiscale numerical simulation, *Appl. Therm. Eng.* **275**, 126690 (2025)

[4] L. Wei, G. Bois & V. S. Nikolayev, Direct numerical simulation of micro-layer dynamics with micro-region modeling in nucleate boiling, *12th International Conference on Multiphase flow,* Toulouse, France (2025)

The Life and Death of Soap Films

Lorène Champougny[1], Jonas Miguet[1], Marina Pasquet[1], Laurie Saulnier[1], Victor Ziapkoff[1], François Boulogne[1], Isabelle Cantat[2], Dominique Langevin[1], Frédéric Restagno[1], Anniina Salonen[1], Benoît Scheid[3], Emmanuelle Rio[1]

[1]*Laboratoire de Physique des Solides, UMR 8502, CNRS, Université Paris-Saclay, 91405 Orsay, France.*

[2]*Univ Rennes, CNRS, IPR (Institut de Physique de Rennes) - UMR 6251, F- 35000 Rennes*

[3]*TIPs – Fluid Physics Unit, Université Libre de Bruxelles C.P. 165/67, 1050 Brussels, Belgium.*

Soap films are fragile objects that become thinner over time before breaking when they become too thin. In this talk, I'll demonstrate the importance of the presence of surfactants, i.e. soap molecules in films... of soap. The very existence of a soap film, stable for several tens of seconds, is due to the presence of surfactant molecules that enable the existence of surface tension gradients compensating for their weight. It is this balance that allows us to describe the profile of a vertical film[1]. The ability of surfactants to maintain surfactant gradients, known as surface elasticity, is also responsible for the thickness of young films, from the moment they are generated[2]. With regard to film thickness over time, it is somewhat counter-intuitive that the nature of the surfactant has very little effect on the flow of the liquid it contains. However, it can have a drastic effect on evaporation[3]. This is the case when glycerol is added to films, whose lifetime can be extended by 1 to 2 orders of magnitude[4] [4]. It has also been observed that black films with a thickness of less than 10 nm can be stabilized up to 10 times longer in the presence of salt.

FIG. 1. Photographies of metric soap films as (left) Lab experiment and (right) artist performance.

[1] Pasquet, M., Restagno, F., Cantat, I., & Rio, E.. Thickness profiles of giant soap films. *Physical Review Fluids*, *8*(3), 034001, 2023.

[2]Champougny, L., Scheid, B., Restagno, F., Vermant, J., & Rio, E, Surfactant-induced rigidity of interfaces: a unified approach to free and dip-coated films. *Soft matter*, *11*(14), 2758-2770, 2015.

[3] M Pasquet, F Boulogne, J Sant-Anna, F Restagno, E. Rio, The impact of physical-chemistry on film thinning in surface bubbles, *Soft Matter*, **18**(24) 2022

[4] M Pasquet, F Boulogne, F Restagno, E Rio, Lifetime of vertical giant soap films: role of the relative humidity and film dimensions, *Soft Matter* 20 (10), 2374-2380, 2024.

Fluid viscoelasticity affects interfacial instability in coflow systems

Ashis Kumar Sen, T Sujith, Shamik Hazra, Lokesh Malik

Department of Mechanical Engineering, IIT Madras, Chennai 600036, Tamil Nadu, India, ashis@iitm.ac.in

Understanding interfacial instability in a coflow system is crucial for effectively manipulating small objects in microfluidics. While previous research has investigated such instabilities in Newtonian systems [1-2], the influence of viscoelasticity on coflow dynamics remains unexplored. To bridge this gap, we present a comprehensive experimental and theoretical analysis of interfacial instability in stratified coflows of Newtonian and viscoelastic fluids within microfluidic confinements.

We categorize the system's behavior into two distinct regimes: stable, characterized by a flat interface, and unstable, which manifests as either a wavy interface or droplet formation, as illustrated in Fig. 1. To systematically identify these regimes, we develop a comprehensive regime plot based on the capillary numbers of the phases [3]. Through linear stability analysis, we determine the complex wave speed and dispersion relation, providing critical insights into the onset and progression of instabilities. By isolating the effects of viscosity and elasticity, we demonstrate that elastic stratification can either stabilize or destabilize the interface, depending on the specific fluid and flow parameters.

Notably, our study reports droplet formation even at high capillary numbers across various Newtonian and viscoelastic coflow systems. The interaction between viscosity and elasticity governs the transition between wavy and droplet-forming instabilities, uncovering a novel mechanism for modulating interfacial behavior. Our findings enhance the understanding of interfacial dynamics in viscoelastic multiphase flows and introduce a new approach for actively controlling instability modes. These insights may find practical applications in microfluidic droplet generation, particle manipulation, and the development of tunable fluid interfaces for lab-on-a-chip systems.

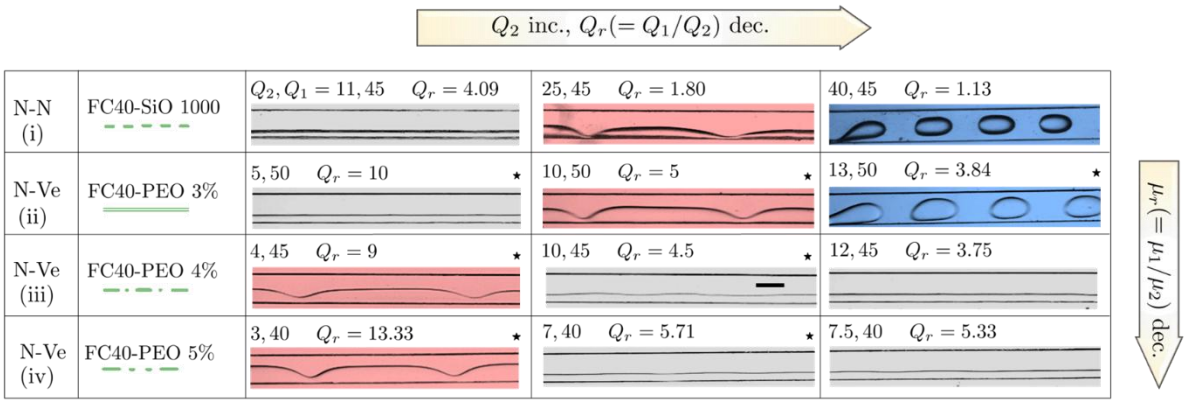

FIG. 1. Experimental images of different regimes: stable (gray), unstable-waviness (red), and unstable-droplet (blue) are shown in a tabular form for varying flow rate ratios (Q_r) and viscosity ratios (μ_r).

[1] R. Govindarajan and K. C. Sahu, *Instabilities in viscosity-stratified flow,* Annual Review of Fluid Mechanics **46** (1), 331‑353 (2014)

[2] A. S. Utada, A. Fernandez-Nieves, J. M. Gordillo, and D.A. Weitz, *Absolute instability of a liquid jet in a coflowing stream*, Physical review letters **100**(1), (2008)

[3] S. Hazra, L. Malik, T. Sujith, and A. K. Sen, *Interfacial instability in a viscoelastic microfluidic coflow system*, Journal of Fluid Mechanics **1000**, A96 (2024).

Fluid Film flow over a Granular Chain

Kishor Kumar Sarva[a], Tejas G Murthy[b] and Gaurav Tomar[c]

[a]Interdisciplinary Center for Energy Research
Indian Institute of Science Bangalore

[b]Department of Civil Engineering
Indian Institute of Science Bangalore

[c]Department of Mechanical Engineering
Indian Institute of Science Bangalore

Abstract

Dripping flow over a thin fibre with beads (granular chain) finds applications in industrial coating and condensation cooling. Flow over a fiber undergoes instability resulting in the formation of droplets. The spacing between the droplets has been categorized in three regimes, namely, isolated droplet formation, Rayleigh-Plateau and droplet merging (wave) regime. In this study, we show that if an obstruction is placed in the form of a solid bead on the fiber, it introduces droplet mergers thus resulting in modification of the droplet spacing. For multiple beads, fluid film morphology is a function of the bead spacing (see Figure 1). Further, we compare the perturbation in velocity introduced by a single bead and compare it with the simulations performed with similar velocity perturbations applied at the faucet.

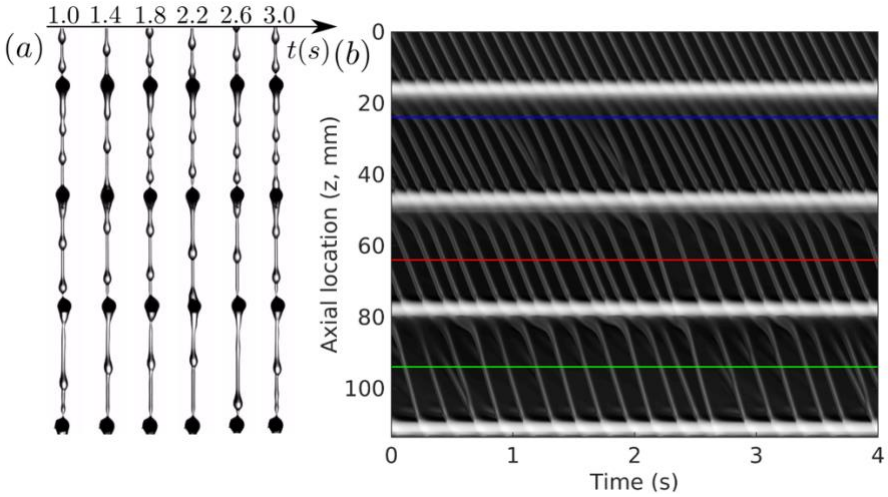

Figure 1: (a) Droplet formation for film flow over a fiber with spherical beads. (b) Spatio-temporal graph showing droplet motion and droplet mergers downstream of beads. We compute the temporal variations in the thickness of the film at axial locations marked by blue, red and green lines.

Bacterial Suspension Flow in Porous Media

Harold Auradou[1]

[1] *Laboratoire FAST, Université Paris-Saclay, CNRS, 530 André Rivière 91405 Orsay, France*
harold.auradou@cnrs.fr

Bacteria possess flagella, which allow them to move within their fluid environment. Physicists consider these biological entities as active particles which inject energy at small scales. These systems have opened a new fertile filed of research related to non-equilibrium physics. From the swimming of a population of bacteria, emerge at large scales, interesting properties of the fluid, such as the appearance of coherent dynamic structures [1], unidirectional flows [2], active motion of small objects and dynamical clustering of passive particles [3].

This presentation will examine the swimming behavior of bacteria in a flow and its impact on dispersion within a porous medium. Our experimental, numerical, and theoretical findings reveal the existence of an "active filtration regime", which enhances the retention of bacteria within the porous structure [4, 5] (See Fig. 1).

One of the interesting properties observed in a suspension of bacteria is their ability to reduce the effective viscosity of the suspension when it is subject to a moderate shear. This emergence is due to the fact that the spatially organized stress response generated by the bacteria motion aids the applied shear stress, leading to a decrease in the effective viscosity [6-9]. We will discuss how this phenomenon influences the hydrodynamic dispersion of dense bacterial suspensions in porous media and create Saffman-Taylor active viscous finger (See Fig 1b and [10]).

Finally, we will open the floor to discuss the potential roles of aerotaxis and chemotaxis in bacterial movement through porous environments.

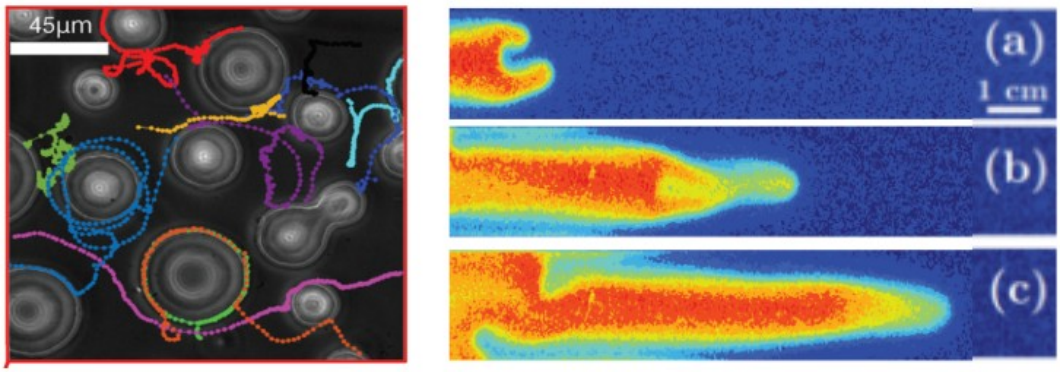

FIG. 1. Left: Colored lines representing trajectories of motile bacteria in the porous space. Hydrodynamic interactions between bacteria and surface traps bacteria causing active trapping. Right: Normalized bacterial volume fraction fields for an experiment in Helle Shaw cell of width W = 2 cm and aperture 500µm. The volume fraction of bacteria in the injected fluid is above the volume fraction from which the effective viscosity of the fluid is zero. The images are taken 30 min apart.

III. REFERENCES

[1] A. Sokolov and I. S. Aranson, Physical Review Letters, 109:248109 (2012).
[5] H. Wioland, F. G. Woodhouse, J. Dunkel, J. O. Kessler, and R. E. Goldstein, Physical Review Letters, 110:268102 (2013).
[3] J. Bouvard, F. Moisy, and H. Auradou, Physical Review E, 107(4):044607 (2023).
[4] A. Creppy, E. Clément, C. Douarche, V. D'Angelo & H. Auradou, Phys. Rev. Fluids 4, 013102 (2019).
[5] M. Dentz, A. Creppy, C. Douarche, E. Clément and H. Auradou, J. Fluid Mech. (2022), vol. 946, A33.
[6] H. M. Lopez, J. Gachelin, C. Douarche, H. Auradou and E. Clément, Phys. Rev. Lett. 115(2):028301 (2015).
[7] A. Ganesh, C. Douarche, M. Dentz, and H. Auradou, Phys. Rev. Fluids, 8:034501 (2023).
[8] V. A. Martinez, et al, Proceedings of the National Academy of Sciences, 117(5):2326– 2331 (2020).
[9] J. Y. Y. Chui, C. Douarche, H. Auradou, and R. Juanes, Soft Matter, 17(29):7004–7013 (2021).
[10] A. Ganesh, C. Douarche, H. Auradou, Phys. Rev. Lett. 134, 128301 (2025).

Microrhology of Real and Artificial Biofluids at the Mesoscale helping Pathogenesis

Dipankar Bandyopadhyay

Professor, Department of Chemical Engineering & Centre for Nanotechnology, Indian Institute of Technology Guwahati, dipban@iitg.ac.in

Abstract

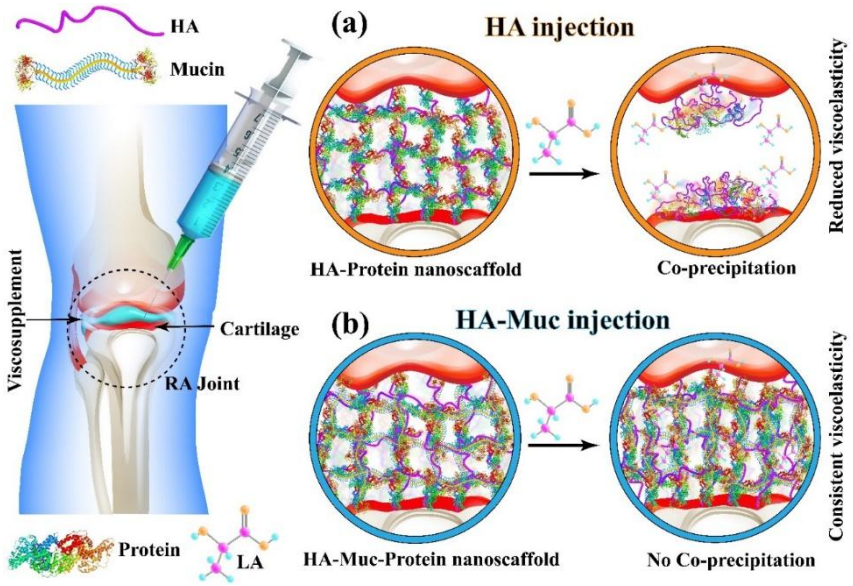

Microrheology of biofluids play an important role in the functioning of the human beings in a daily life. While the tear films on the eyes act as an excellent protective layer cum lubricant, the synovial fluids at the bone or cartilage joints help in diverse mobility aspects of the human body. In this talk, we analyse a set of very interesting biofluids such as mucin, synovial fluids, and extracellular matrix to study their microrheological behaviours before developing in-vitro bioengineering model to artificially analyse their efficacy. In the process, we shall also explore the variations in their viscous, elastic, and relaxational properties of such biofluids during the transformation from the healthy to the diseased states to uncover the microrheological reasons behind the disease onsets. For example, thickening of saliva as a protection to the pathogens, cystic fibrosis in the mucus linings, immobilization of joints due to the thickening or degeneration of the synovial fluids, among others. In the process, we shall also 'sightsee' the translational aspects of the study to develop artificial synovial fluids with similar efficacy as the biological ones.

Keywords: Microrheology, biofluids, mucin, synovial fluid, extracellular matrix

Cruising and jumping, the dynamic behaviour of micro-swimmers in turbulence

E. Climent[*], F.-G. Michalec[+], O. Praud[*], M. Lorite-Diez[*], S. Cazin[*], and S. Souissi[+]
[*] *Institut de Mécanique des Fluides de Toulouse, CNRS, Toulouse INP, Univ. Paul Sabatier – Toulouse, France.*
[+] *Laboratoire d'Océanologie et de Géosciences, CNRS, Univ. Lille, ULCO – Wimereux, France.*

I. CONTEXT AND OBJECTIVES

Plankton are small organisms that are by definition carried along by ocean currents. However, many species do not behave as passive particles and propel themselves with velocities ranging from 10 to 1000mm/s. Turbulence is a ubiquitous feature of marine ecosystems which affects the spatial distribution of plankton[1], their behaviour, their ability to obtain food or locate a partner, which in turn influences ecosystem-scale processes. Copepods (planktonic crustaceans) make up most of the biomass in the oceans and are a major food source for fish. They alternate phases of active (jumping) and passive (cruising) transport[2]. These behavioural responses to flow are still largely unknown due to a complex coupling between hydrodynamic forces and the morphology of the organisms (size close to the dissipative scale[3], non-spherical shape, and density different from that of the fluid).

II. EXPERIMENTAL SETUP

All our experiments were carried out in a rectangular glass tank with dimensions 0.4 m×0.4m×1.2m (see Fig 1a) filled with salted water at 18°C (salinity 15, density $\rho_f = 1.01$ g/cm^3). The turbulent flow is generated by the vertical oscillation of two horizontal grids located 40cm apart. The grids are made of square bars often used in wind tunnels for generating isotropic homogeneous turbulence. The grids, attached to a motorized linear slide, oscillate at frequency f=2Hz with a maximum stroke equal to 80mm. Fluid and copepods dynamics is simultaneously recorded using a stereovision system composed of four synchronized Phantom VEO 640L cameras recording images with a spatial resolution of 2560×1600 pixels. The illumination is provided by a high-power dual cavity laser (Photonics Industries DM60-527-DH 2x60mJ @ 1kHz). The volume of interest (VOI) is defined as a rectangular volume of 200mm×150mm×100mm located at equal distances from the two grids. The large dimensions of the VOI make it possible to track a large number of copepod trajectories over a long period of time (fig. 1b). To characterize the flow, the water is seeded with spherical (20 mm diameter) polyamide particles. Before each measurement, copepods were gently transferred from the culture vessels to the experimental water tank where they acclimate for one hour. The number density is approximately 400 copepods per litre which is similar to values observed in estuaries.

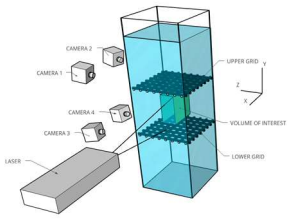

Figure 1a: Volume of interest between the two mobile grids.

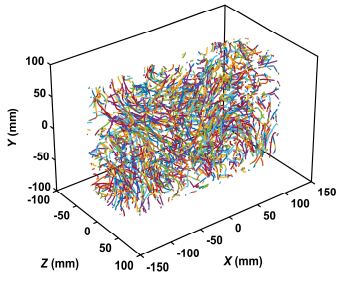

Figure 1b: Trajectories of copepods swimming in a turbulent flow.

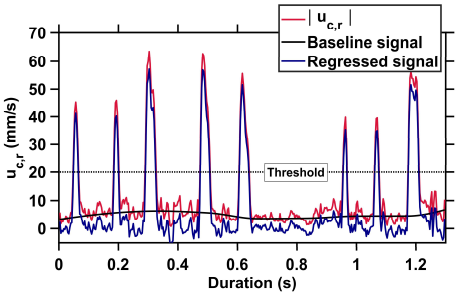

Figure 1c: Time series of the copepod relative velocity and threshold to detect jumps.

III. RESULTS

Fluid tracers and copepods trajectories are reconstructed by means of 3D Lagrangian particle tracking velocimetry (Lavision Shake-the-Box algorithm) allowing tracking at high seeding concentration. To disentangle copepod dynamics from the underlying turbulence fluctuations, one needs to consider their relative motion (Fig. 1c) with respect to the carrier fluid and use a threshold for jump detection: the relative velocity is defined as $\mathbf{u}_{c,r}(t) = \mathbf{u}_c(t) - \mathbf{u}_f(\mathbf{x}_c(t), t)$, where $\mathbf{u}_c(t)$ is the copepod velocity and $\mathbf{u}_f(\mathbf{x}_c(t), t)$ is the local instantaneous flow velocity at the copepod position. Statistical properties (jump amplitude and duration) are used to characterize the interactions of copepods with turbulence. We find out that the mean jump amplitude decreases very slightly from 48mm/s in calm water to 40mm/s in a turbulent flow and that average jump duration also decreases slightly from 0.028s in calm water to 0.021s in a turbulent flow. However, the jump frequency increases from 0.66Hz in calm water to 0.93Hz.

This 40% increase indicates that copepods are able to adjust their swimming effort to the ambient flow by jumping more frequently while maintaining the other characteristics of their motion. Experiments with copepods exposed to microplastics (6-7 mm plastic debris) have shown that these statistics vary significantly as a signature of the toxicity of microplastic particles ingested by copepods.

[1] Ardeshiri et al. *Phys. Rev.* E **93** (4), 043117 (2016).
[2] Michalec et al. *PNAS* **114** (52), E11199 (2017).
[3] Michalec et al. *Eur. Phys. J. E* **45** (2), 12 (2022).

Deep-Lung Anatomical Model Reveals Pulmonary Surfactant's Role in Easing Respiratory Distress

Isabella Francis[1], Suvash C. Saha[1,*], Philip M. Hansbro[2], Dhruba Dhar[3], Mohammad Z. Islam[4], Suman Chakraborty [5]

[1]School of Mechanical and Mechatronic Engineering, Faculty of Engineering and Information Technology, University of Technology Sydney, NSW, Australia
[2]Centre for Inflammation, Centenary Institute & University of Technology Sydney, School of Life Sciences, Faculty of Science, Sydney, New South Wales 2050 & 2007, Australia
[3]School of Medical Sciences & Technology, Indian Institute of Technology Kharagpur, Kharagpur, 721302, West Bengal, India
[4]Department of Mathematics, Jashore University of Science and Technology, Jashore-7408, Bangladesh
[5]Department of Mechanical Engineering, Indian Institute of Technology, Kharagpur 721302, India

ABSTRACT

Pulmonary diseases leading to respiratory distress syndromes are profoundly influenced by the interplay between interfacial tension at the alveoli and fluid flow-induced stresses in the airways. These factors are further shaped by the anatomical structure of the pulmonary pathways and their unique deformation under airflow, serving as a personalized signature of an individual's respiratory health. Despite extensive research on deep lung airflow dynamics, a clear understanding of the relationship between flow-induced lung damage and alveolar surface tension remains grossly elusive. To address these challenges, we establish a quantitative link between airway blockage, pulmonary flow dynamics within the hierarchical lung structure, and interfacial tension at the alveolar linings. This is achieved through in-silico simulations using a branched fluidic network model that replicates physiological conditions, complemented by advancing a biomimetic lung-on-a-chip model on an artificially engineered platform. Furthermore, by examining the interaction between surfactant drug molecules and alveolar mucus, we propose a predictive approach for assessing surfactant-drug therapy efficacy. This approach integrates patient-specific anatomical and physiological characteristics, laying the groundwork for a personalized strategy in pulmonary disease management, in contrast to conventional empirical and experience-based methods.

Fluid mechanics in the human body : tear-film, cerebrospinal fluid flows and mucociliary clearance

Anjishnu Choudhury[1]

[1] *Department of Mechanical Engineering, IIT Bombay, India* a.choudhury@iitb.ac.in

The mechanics of biological transport processes is very complex. In addition to fluid rheology, the geometry, complex kinematics and coupled multi-physics frequently come into play. Here, I will talk about such complex biological fluid mechanics problems. There is an emerging and promising area of bio-fluid mechanics where a variety of biological mechanisms can be modelled and explained using fluid dynamical principles. Current problems being pursued in the group related to fluid dynamics in the human body are: (i) tear-film instability due to bacterial infection, (ii) cerebrospinal fluid (CSF) flow modelling in the brain ventricles; and (iii) mucus transport modelling in pulmonary airways. These studies will help in building better understanding of biological fluid flows in the human body using fluid mechanical principles and can potentially contribute to the calibration and invention of medical diagnostic devices. For the scope of this talk, I will discuss the first two topics.

I. SHORTENING OF BREAK-UP TIMES OF HUMAN TEAR-FILMS

Evaluating break-up time (BUT) of tear films is of great importance in diagnosis of dry-eye disease. Clinical studies have reported inhomogeneous concentrations of mucin across the bulk of the tear-film in dry-eye disease, as shown in fig. 1. This is thought to be one of the prime reasons for severe shortening of BUTs[1]. We have modelled such mechanisms, specifically heterogeneous membrane associated mucins (MAMs) using fluid dynamical concepts such as negative slip at the corneal epithelium and enhanced van-Der Waals interactions[2], showing severe shortening of BUTs.

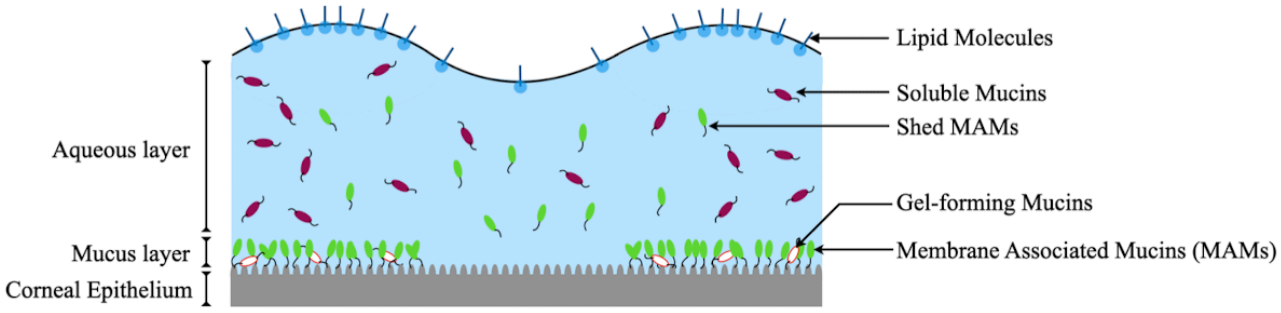

Figure 1: Schematic of a tear-film

Currently, in collaboration with Dinesh B. (IIT(BHU) Varanasi, India) and H. Dixit (IIT Hyderabad, India), we are formulating a realistic model of bacterial effects on MAMs based on concepts of population dynamics coupled with thin film mechanics. This will improve upon our earlier study where the heterogeneity was prescribed *a priori*. In this new approach, the heterogeneity of MAMs will emerge naturally due to a perturbation in bacterial concentration.

---

[1] Dey, M., Vivek, A. S., Dixit, H. N., Richhariya, A., & Feng, J. J. (2019). A model of tear-film breakup with continuous mucin concentration and viscosity profiles. *Journal of Fluid Mechanics*, *858*, 352-376.

[2] Choudhury, A., Dey, M., Dixit, H. N., & Feng, J. J. (2021). Tear-film breakup: The role of membrane-associated mucin polymers. *Physical Review E*, 103(1), 013108.

II. CEREBROSPINAL FLUID FLOW MODELLING

Understanding the Cerebro-Spinal Fluid (CSF) flow and its role in transporting metabolites across the blood-brain barrier has important implications for human health[3]. For example, many neurodegenerative disorders are thought to correlate with unwanted accumulation of natural waste macromolecules like amyloid beta protein in Alzheimer's disease. An unhealthy accumulation of CSF in the skull, known as hydrocephalus, can result in headaches and mental impairment. It can be caused by displacement of tissue in the cerebellum and/ or blockage of the cerebral aqueduct which is a narrow passage between the brain ventricles. Although medical symptoms and biological causes are an active area of research, the physical modelling of the flow

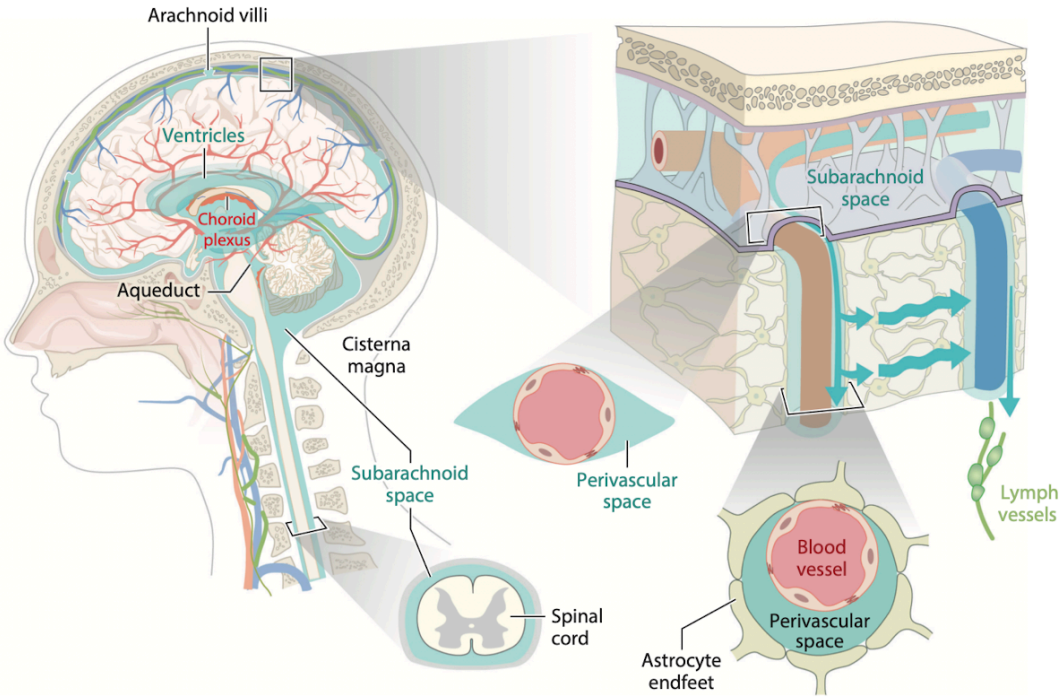

Figure 2. Anatomy of the glymphatic system with focus on the perivascular spaces in the subarachnoid space and brain tissue[3].

system is scarce and merits detailed investigation. Fig. 2 shows the aqueduct in the ventricular system (not shown) and a blown up schematic of the *glymphatic* system showing the perivascular space.

We aim to explore the modelling of CSF flows in diseased conditions at two different length-scales relevant to two distinct diseases: (i) CSF flows in the ventricular chambers. This is relevant for modelling conditions like hydrocephalus. (ii) CSF flows in perivascular and interstitial spaces. This study will be at a much smaller length-scales, modelling flows across porous media inside the brain tissue. The complexities of the modelling strategy include identification of the relevant geometry for the concerned disease, correct boundary conditions and correlation of biomedical data to fluid dynamical parameters.

[3] Kelley, D. H., & Thomas, J. H. (2023). Cerebrospinal fluid flow. *Annual review of fluid mechanics*, 55(1), 237-264.

Microfluidic Oxygenator for Artificial Lung Applications: Toward Bioinspired Gas Exchange at the Microscale

Julie Lachaux[1], Gilgueng Hwang[1,2], Nassim Arouche[3], Sina Naserian[3], Abdelmounaim Harouri[1], Valeria Lotito[1], Caterina Casari[4], Thevy Lok[5], Jean Baptiste Menager[6], Justin Guihaire[6], Cécile V. Denis[4], Peter J. Lenting[4], Abdul Barakat[5], George Uzan[3], Olaf Mercier[6] and Anne-Marie Haghiri-Gosnet[1]

[1] Université Paris-Saclay, CNRS, C2N, UMR9001, Palaiseau 91120, France
[2] LIMMS, CNRS, The University of Tokyo, Tokyo, Japan (current position)
[3] Université Paris-Saclay, INSERM, UMR-S-MD 1197, Hôpital Paul Brousse, Villejuif, France
[4] Université Paris-Saclay, INSERM, UMR S1176, Le Kremin-Bicêtre, France
[5] LadHyX, CNRS, Ecole polytechnique, Institut polytechnique de Paris, Palaiseau 91120, France
[6] Université Paris-Saclay, INSERM UMR_S 999 "Pulmonary Hypertension: Pathophysiology and Novel Therapies", Hôpital Marie Lannelongue, Le Plessis-Robinson, France

We present a microfluidic oxygenator designed to replicate the gas exchange function of the human lung in a compact and efficient format (Fig. 1). This bioinspired system integrates microchannel networks that facilitate controlled gas-liquid interface dynamics, mimicking alveolar structures and enabling effective oxygen and carbon dioxide exchange.

The device architecture is optimized for high surface-area-to-volume ratio and minimal diffusion distances, allowing for efficient gas transfer while minimizing hemolysis and shear stress. Fabrication techniques ensure precise control over channel geometry and membrane integration. Initial results demonstrate stable and continuous gas exchange under physiologically relevant flow conditions.

This microfluidic approach offers a promising pathway for developing next-generation artificial lungs, with potential applications in extracorporeal life support and long-term respiratory assistance. The platform also provides a versatile tool for studying pulmonary physiology and testing respiratory therapies at the microscale.

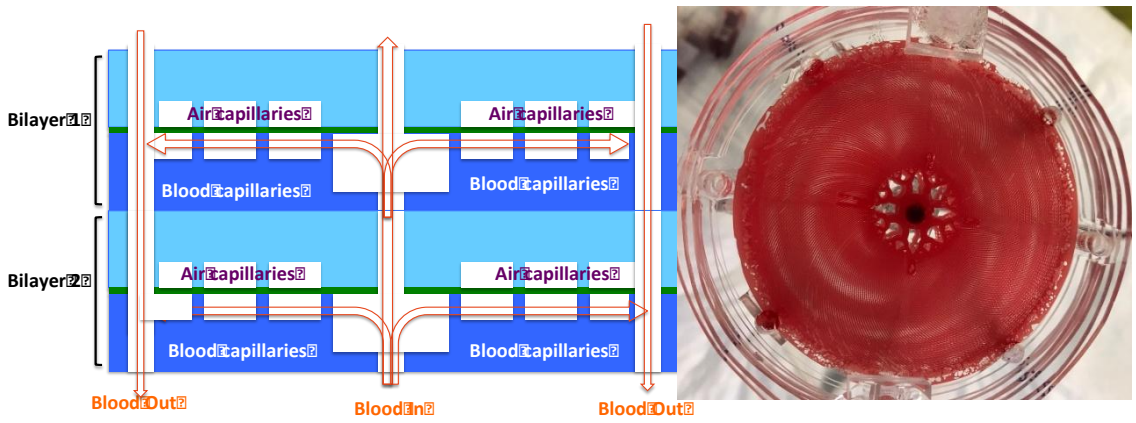

FIG. 1. Proposed microfluidic oxygenator. Left: vertically stacked architecture; Right: fabricated microfluidic oxygenator.

[1] A-M. Haghiri-Gosnet, Lyas Djeghlaf, Julie Lachaux, Alisier Paris, Gilgueng Hwang, European Patent EP18306405.4 (29 Oct. 2018) "Microfluidic gas exchange devices and methods for making same"

[2] J. Lachaux, G. Hwang, N. Arouche, S. Naserian, A. Harouri, V. Lotito, C. Casari, T. Lok, J-B. Menager, J. Issard, J. Guihaire, C. V. Denis, P. J. Lenting, A. I. Barakat, G. Uzan, O. Mercier, A.M. Haghiri-Gosnet, "A compact integrated microfluidic oxygenator with high gas exchange efficiency and compatibility for long-lasting endothelialization", Lab on a Chip **21**, 4791-4804 (2021).

Phase separation of red blood cell suspension on filter paper: healthy vs pathological cases

Sampad Laha[1], Ananta Kumar Nayak[1], Alexander Farutin[1], Suman Chakraborty[2], Chaouqi Misbah[1]
[1] *University of Grenoble Alpes, CNRS, LIPHY, F-38000, Grenoble, France.*
chaouqi.misbah@univ-grenoble-alpes.fr
[2] *Department of Mechanical Engineering, Indian Institute of Technology, Kharagpur, India-721302.*
suman@mech.iitkgp.ac.in

Physiological properties of red blood cells (RBCs) may vary drastically in certain diseased conditions, causing a significant impact on their corresponding migration tendencies [1]. In this work, we have used certain chemicals (macromolecules and enzymes) to alter some of the mechanical and functional properties of the RBCs (in order to mimic some specific diseased conditions) and studied the spreading of suspensions of these chemically treated cells through laboratory filter paper (average pore size ~ 11 μm). Simple DSLR videography and image analysis have been used to demonstrate the effect of varying aggregability, membrane deformability and altered glycocalyx properties on the wicking dynamics of the RBC suspension, highlighting the emergence of distinct phase separation regimes between the liquid and cellular matter. It is found that for a particular porous confinement, phase separation is strongly influenced by the cellular volume fraction and the degree of cellular aggregation (as shown in FIG. 1). In order to decipher the effect of RBC membrane deformability on the phase separation phenomenon, wicking experiments have been carried out with suspension of RBCs artificially rigidified with 0.1% glutaraldehyde solution. Rigid cell suspensions have shown wide spread phase separation for a broad range of cellular volume fractions as well as dextran concentrations, unlike deformable healthy samples. Another key aspect that we have investigated is the effect of enzymatic glycocalyx degradation on the wicking characteristics of cellular suspensions through paper, with an aim to understand the impact of the glycocalyx layer on underlying the wicking mechanism and cellular aggregation. Our observations pertaining to phase separation are qualitatively supported by numerical predictions of RBC transport through a heteronomous porous media with random circular obstacles simulated using Immersed Boundary Lattice Boltzmann framework. These phase separation regimes may not only be interesting from fundamental scientific point-of-view, but can also act as important markers for screening samples with abnormal cellular properties and diseased conditions through the use of paper-based point-of-care diagnostic devices [2].

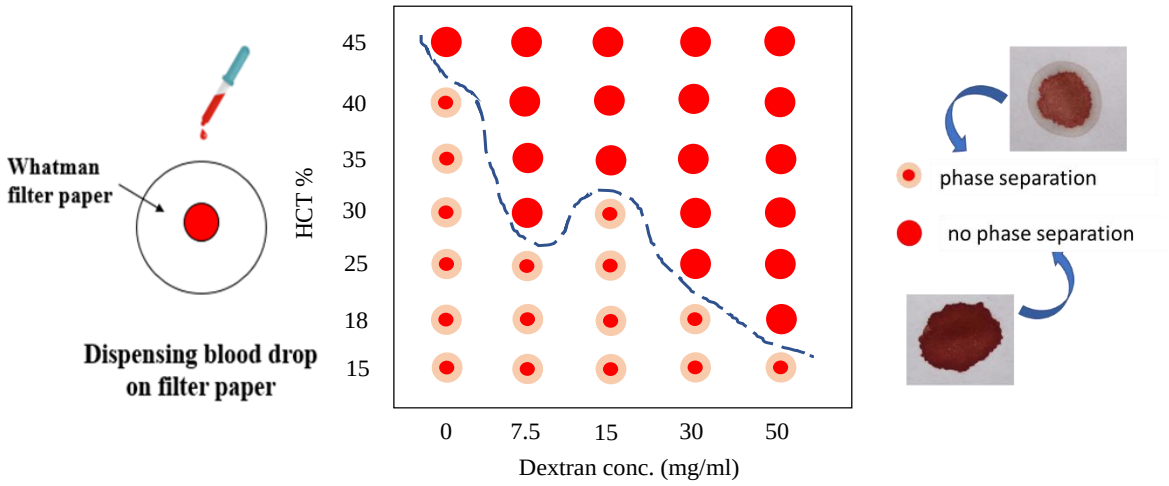

FIG. 1. Regime diagram showing the effect of aggregability on the threshold HCT for phase separation of RBC-PBS suspensions having different dextran concentrations. Inset figures show representative experimental images of phase separation on filter paper.

[1] Tomaiuolo, G. "Biomechanical properties of red blood cells in health and disease towards microfluidics." Biomicrofluidics 8(5), 051501, (2014).
[2] Laha, S., Bandopadhyay, A. and Chakraborty, S., Smartphone-integrated label-free rapid screening of anemia from the pattern formed by one drop of blood on a wet paper strip. ACS sensors, 7(7), pp.2028-2036, (2022).

Mucus dynamics and aerosol transport in lung airways

Swarnaditya Hazra[1] and Jason R. Picardo[2]

[1] *Department of Chemical Engineering, IIT Bombay, 400036, Mumbai, India* swarnaditya9791@gmail.com

[2] *Department of Chemical Engineering, IIT Bombay, 400036, Mumbai, India* picardo@iitb.ac.in

This talk will address three central questions in pulmonary fluid mechanics: (a) When do mucus films plug airways? (b) What is the distribution of mucus in open airways and how does this impact the deposition of inhaled aerosols (c) What, if any, is the role of cilia in maintaining a stable film and an open airway? Our work is based on the reduced-order, thin-film model of Dietze and Ruyer-Quil [1], which is used to describe the dynamics of the mucus-air interface, as well as the flow in both phases. Mucociliary transport is incorporated via a coarse-grained boundary condition at the base of the mucus film (Fig. 1a). In addition, the transport of a range of particles (0.1 to 50 microns) is modelled using the Maxey-Riley equation, augmented with Brownian forces.

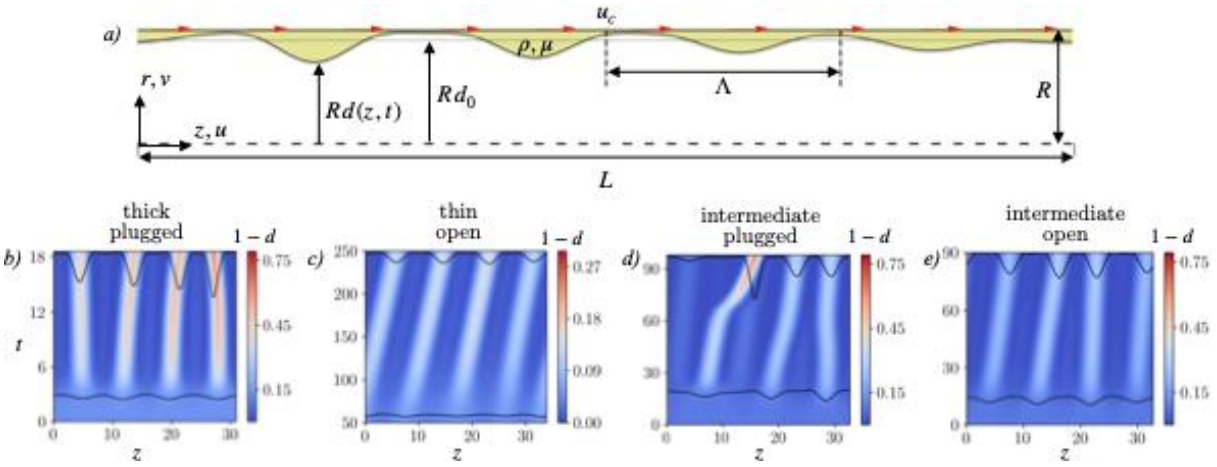

FIG. 1. (a) Schematic of the mucus film in a ciliated airway. (b-e) Illustrative examples of the film's evolution.

First, using a large ensemble of simulations of randomly perturbed films, we will show that the answer to when plugs form is not determined by just the film's volume. While very thick films always plug (Fig 1b) and very thin films always stay open (Fig. 1c), we find a range of intermediate films for which plugging is uncertain [2]. This probabilistic nature arises due to the spontaneous axial sliding of growing humps – a lucky hump can sweep up a disproportionate share of the film's volume and so form a plug (Fig 1d-e).

Next, focusing on open airways, we ask whether inhaled aerosols can avoid the mucus film and deposit on the airway wall -- an outcome that is harmful in case of allergens and pathogens but beneficial in case of aerosolized drugs. The Rayleigh-Plateau instability continues to play an important role, by drawing the mucus into large annular humps and leaving substantial areas of the wall exposed to particles. Our simulations reveal a non-monotonic dependence of deposition on particle size, as Brownian forces give way to inertial forces. Remarkably, we find that increasing the mucus volume need not increase particle entrapment; rather, the effect depends on particle-size [3].

Finally, we will replace the periodic boundary conditions used in most studies by open-domain conditions, which allow for a continuous supply and clearance of mucus. Though numerically challenging, this setting enables us to elucidate the role of cilia in maintaining open airways.

[1] G. F. Dietze and C. Ruyer-Quil, Films in narrow tubes, J. Fluid Mech. 762, 68 – 109 (2015).

[2] S. Hazra and J. R. Picardo, Probabilistic plugging of airways by sliding mucus films, arxiv.org/abs/2504.01656 (2025).

[3] S. Hazra and J. R. Picardo, Aerosol deposition in mucus-lined ciliated airways, arxiv.org/abs/2502.01883 (2025).

Microfluidic insights into amyloid aggregation

Gaëlle Audéoud [1, 2], Maxime Lavaud [1, 2, 3], Lucie Khemtermourian [2], Yacine Amarouchene [1],

Marion Mathelié [2], Thomas Salez [1]

[1] Laboratoire Ondes et Matière d'Aquitaine, 33400, Talence, France,
[2] Institute of Chemistry & Biology of Membranes & Nano-objects, 33600, Pessac, France
[3] Universität Wien, Boltzmanngasse 5, 1090, Wien, Austria

Amyloid proteins are widespread in nature, from human to bacterial cells, and are characterized by their ability to aggregate into ordered fibrils that are notably the hallmark of protein-aggregation disorders (e.g. Alzheimer disease [1]). Amyloid fibrillation is a dynamic and environment-dependent process with dynamic exchange between the initial monomers, the intermediate oligomers and the end-products, i.e. the fibrils, each displaying particular properties associated to different biological activities. In the aim of understanding aggregation and specially to quantify the size distribution of fibrils, we developed a microfluidic experiment based on the Taylor-dispersion analysis [2]. This method presents the advantages of being quick (few minutes of measurements), not altering the proteins by the addition of tracers and being applicable to other polydisperse solutions or suspensions.

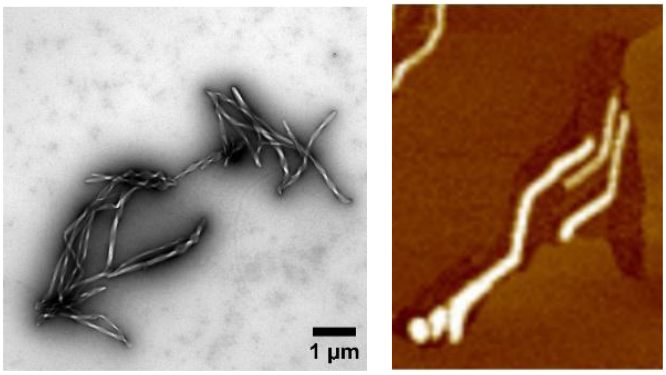

FIG. 1. Amyloid proteins tend to form long and thin aggregates named fibers. Left: PSMα3 fiber; Right: Membrane perforation. Image from Marion Mathelié.

[1] A.Nordberg, *PET imaging of amyloid in Alzheimer's disease,* The Lancet Neurology (2004).
[2] H.Cottet et al, *Taylor Dispersion Analysis of Mixtures*, Analytical Chemistry (2007).

New strategy of cancer treatment combining metallic nanoparticles with radiation therapies

Sandrine Lacombe[1] and Erika Porcel[2]

[1] *Institut of Molecular Sciences Orsay, 91405, Orsay, France*

Radiotherapy is used for 50% of the cancer treatments. Despite important technological improvements, secondary effects remain significant due to lack of tumor selectivity and potential radioresistance.

A new strategy combining radiation with tumor targeted nanoagents to improve tumor diagnostic and therapeutic index of radiations, has emerged. The potential of theranostic nanoparticles to improve the performances of radiotherapy and hadrontherapy will be presented. These agents are produced with an original method based on a radiolytic process [1]. The principle of radioenhancement effect has been evidenced at molecular and cellular scales. Experiments in vivo shows their efficacy as contrast agents for CT and TEP medical imaging [2].

New methods and models are developed to identify potential toxic effects of nanoparticles in blood [4] and to rapidly evaluate the efficiency of amplification prior to preclinical experiments [3].

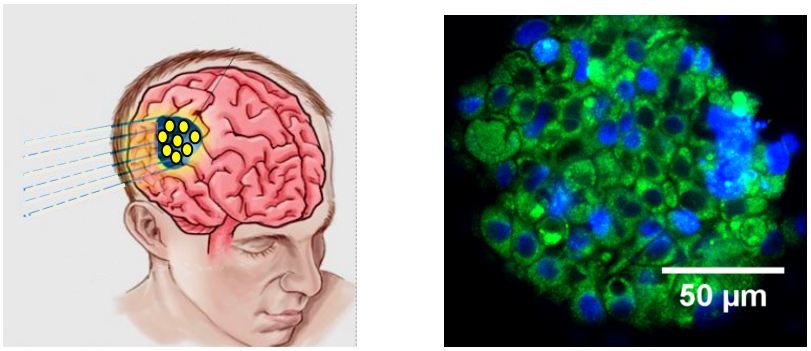

FIG. 1. Left: Principle of NP combined particle therapy. Right: NPs in a tumor cell spheroid.

[1] D. Salado-Leza, E Porcel, X. Yang, L Stefancikova, M Bolsa-Ferruz, F Savina, D Dragoe, JL Guerquin-Kern, TD Wu, R Hirayama, H Remita, and S. Lacombe. Green One-Step Synthesis of Medical Nanoagents for Advanced Radiation Therapy, Nanotechnology, Science and Applications 2020, 13, 61-756.

[2] Yang, X.; Tran, V.L.; Remita, H.; Savina, F.; Denis, C.; Kereselidze, D.; Jego, B.; Lacombe, S.; Porcel, E.; Truillet, C. Pharmacokinetics derived from PET imaging of inspiring radio-enhancer platinum nanoparticles. Nanomedicine: Nanotechnology, Biology, and Medicine 46 (2022) 102603. DOI: 10.1016/j.nano.2022.102603

[3] Yang, X.; Porcel, E.; Marichal, L.; Gonzalez-Vargas, C.; Khitous, A.; Salado-Leza, D.; Li, X.; Renault, J.-P.; Pin, S.; Remita, H. et al. And S. Lacombe. Human Serum Albumin in the Presence of Small PlatinumNanoparticles Journal of Pharmaceutical Sciences 2024. DOI: 10.1016/j.xphs.2024.02.002

Elasticity from contacts in branched actin

Mehdi Bouzid,[1, 2] Cesar Valencia Gallardo,[3] Magdalena Kopec,[3] Lara Koehler,[1, 4] Giuseppe Foffi,[5] Olivia du Roure,[3] Julien Heuvingh,[3] and Martin Lenz[1, 3]

[1] *Université Paris-Saclay, CNRS, LPTMS, 91405, Orsay, France*
[2] *Université Grenoble Alpes, CNRS, 3SR, 38400 Saint Martin d'Hèeres, France*
[3] *PMMH, CNRS, ESPCI Paris, PSL University, Sorbonne Université, Université Paris-Cité, F-75005, Paris, France*
[4] *Max Planck Institute for the Physics of Complex Systems, Dresden, Germany*
[5] *Université Paris-Saclay, CNRS, LPS, 91405, Orsay, France*

The biologically crucial elasticity of actin networks is usually understood as an interplay between the bending and stretching of its filaments. This point of view however fails when applied to the weakly coordinated branched actin networks found throughout the cell. Through experiments and theory, we show that their elasticity crucially involves reversible contacts between their filaments. These contacts can in turn be controlled through filament entanglement during network growth to regulate the final properties of the network. These properties could be key to understanding how moving cells dynamically adapt their cytoskeleton to their environment.

Droplet/particle movement through constricted passage

Bahni Ray

Department of Mechanical Engineering, IIT,110016, Delhi, India, bray@mech.iitd.ac.in

Pressure-driven droplet flows through a constricted channel either attains a steady shape, undergoes breakup or fragments into smaller droplets over time. This evolution of droplet depends on various physical parameters including capillary number, viscosity ratio, drop size and the geometry of the constricted channel. The constriction dimensions, namely length and depth, alter the deformation of droplet and can induce breakup/fragmentation. Here we examine the effects of constriction shape on droplet deformation and velocity by defining *shape parameter* (k), a dimensionless quantity based on the relative projected area occupied by the constriction. It is seen that a decrease in k increases the drop deformation and elongation. This behavior can be attributed to a higher effective surrounding fluid velocity around the droplet for a lower k compared to a higher k. Understanding this mechanism can help in deciding the constriction shape for droplet motion where breakup is not desired.

In a different scenario particle movement through constricted passage as seen during air filtration through filters, is governed mainly by the adhesive and cohesive forces between the filter material and particles, the particle kinetic energy and the angle of impact. While droplet and particle motion in constricted passage shows different physical mechanism, both are governed by their size, relative velocity and material of the constriction. Due to the mechanism of particle capture in filter media, we observe particles smaller than the constricted passage (pore size) also getting captured.

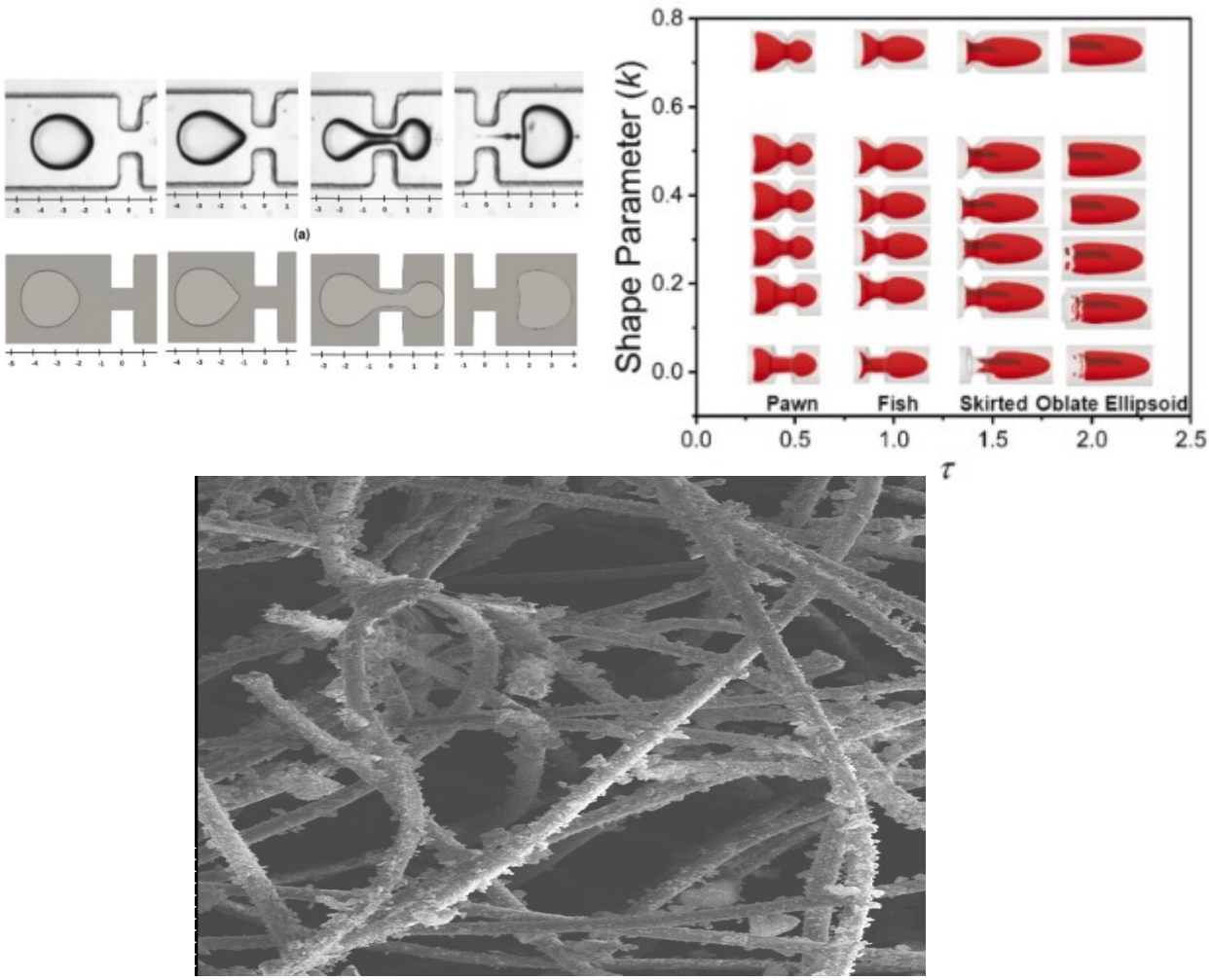

FIG. 1. TOP. Left: Droplet deformation through constricted microchannel for Ca = 0.06, λ = 0.08, η = 1.19, a = 0.64, L = 0.5 and D = 0.75 compared to experiments by Li et al. (2022); Right: Droplet deformation at different time steps for different values of shape parameter, k at D = 0.5 and L = 1 and Ca = 0.5. BELOW: SEM image of particle attached to filter media.

REFERENCES

[1] Z. Li, Z. Gu, R. Li, C. Wang, C. Chen, C. Yu, Y. Zhang, Q. Shu, W. Cao, J. Su, “A geometrical criterion for the dynamic snap-off event of a non-wetting droplet in a rectangular pore–throat microchannel”,Phys. Fluids, 34 (2022).

[2] A Singla, B Mehul, B Ray, “Droplet dynamics in a constricted microchannel”, Chemical Engineering Science, 300 (2024).

[3] A. Singla, B. Ray, “Effects of surface topography on low Reynolds number droplet/bubble flow through a constricted passage” Phys. Fluids, 33 (2021).

Flow of foams in porous media

H. Bodiguel[1], A. Bagaidilov[2], S. Colombano[2], M. Cochennec[2], S. Omirbekov[3], D. Darvazani[2] and L. Oxarango[1]

[1]Univ. Grenoble Alpes, CNRS, Grenoble-INP, France
[2] BRGM, Orleans, France
3 Nazarbayev University, Astana Kazakhstan

In the context of soil remediation, foams are generated and injected into polluted soil to enhance remediation efficiency. The physical origin of this improvement lies in the large pressure gradients created by foam flow, in contrast to water flow, which tends to homogenize the displacement front. The effective viscosity of foam can reach several hundred to several thousand times that of water, depending on the capillary number, *Ca*. It generally increases with the relative gas flow rate, f_g, up to a maximum, beyond which the foam is believed to become unstable. Conversely, it decreases with increasing *Ca*, indicating strong shear-thinning behavior. Although these trends have been reported in various porous media, a comprehensive understanding of these complex flows remains lacking. Moreover, in most experiments, only pressure drops are measured, while direct observations in real or model soils are often difficult or impossible. While the relative gas flow rate and total flow rate are commonly controlled parameters, the gas volume fraction within the porous medium is not directly accessible and may differ from f_g due to flow heterogeneities and gas trapping.

Recent microfluidic approaches that mimic porous media have reproduced the main features of foam flow[1] and revealed that the flow is concentrated along preferential pathways, depending on *Ca* and f_g. The effective viscosity was found to be proportional to f_g/Ca, a behavior interpreted as resulting from quasi-static bubble deformation through constrictions. Extending these observations to three-dimensional systems is of great interest to assess their relevance in more realistic porous media.

In this study, we use a model soil composed of sand grains packed into a column. The column is equipped with pressure sensors, several observation windows, and Time Domain Reflectometry (TDR) sensors. These latter devices allow in situ measurement of water saturation. To our knowledge, this is the first experimental setup that enables simultaneous and direct measurement of both water saturation and pressure gradients.

Results obtained over a wide range of f_g and *Ca* semi-quantitatively confirm in 3D the findings of Mauray et al. regarding the pressure drop induced by foam flow. The water saturation measurements yield striking results: the water fraction remains very low (5–15%), even at low f_g. This strongly suggests that most of the gas phase is trapped within the medium and that the flow is highly heterogeneous.

[1] A. Mauray , M. Chabert, H. Bodiguel, *Phys. Rev. Fluids* 2020

Effect of Porous Metal Packing and Substrate Surface Characteristics on Hydrate Growth

Randeep Ravesh, Sonali Suman, Ayaj Ahamad Ansari, Malay Kumar Das, Pradipta Kumar Panigrahi*

*Department of Mechanical Engineering Department, IIT Kanpur, UP 208016 India *panig@iitk.ac.in²*

Clathrate hydrates play critical role in several gas storage, gas transportation and flow assurance applications. However, slow hydrate formation kinetics remains a bottleneck for the industrial implementation of hydrate based technologies[1]. Present study investigates the influence of reactor bed arrangements using metal packing and surfactants for enhancing methane hydrate formation due to the capillary effect. The experiments were conducted in a large-scale 25 L reactor with different bed configurations at 75 bar initial pressure and 275.15 K reactor temperature. The effects of two surfactants i.e., SDS and Tween 20 were studied. The performance of hydrate formation was evaluated using induction time, hydrate formation kinetics, and hydrate dissociation at constant pressure. Hydrate formation kinetics were also analysed using affinity rate constant and time constant parameters obtained from chemical affinity-based modelling. It is observed that material packings of the reactor bed reduce induction time and enhance hydrate formation kinetics. The hydrate columns as high as 11.6 cm are observed on the surface of packings due to capillary action (see fig 1). The increase in hydrate formation rate can be attributed to the enhanced surface area distributed inside the reactor by the metal packings and the effect of capillary action. The affinity time constant reduces from 17.39 h to 9.98 h for 4 mM SDS concentration with knitmesh packing arrangement**.** The packing arrangement and surfactants also improves the gas recovery during hydrate dissociation justifying the benefits and potential of reactor bed arrangement and surfactants.

Hydrate formation is an interfacial phenomenon, which is affected by the surface characteristics of reactors and pipelines. Therefore, the present investigation reports hydrate formation at the cyclopentane-water interface [2] by placing the water droplet on hydrophobic and hydrophilic substrates submerged in a cyclopentane pool. Experiments were conducted using a 10 μL sessile water droplet at a reactor temperature of 3 °C and atmospheric pressure. The influence of NaCl salt on hydrate growth was studied at 0, 0.5, and 2.0 wt.% concentrations due to the importance of salinity in several hydrate-based applications. There is formation of hydrate fibres, rotational and translational movement during hydrate growth on hydrophobic substrate. However, the lifting of the droplet and generation of hydrate fibres are absent in the case of hydrophilic substrate (see fig 2). The hydrate formation time is lower for hydrophilic substrates than that of hydrophobic substrates. The hydrate formation time also increases with the addition of salt i.e., there is increase of 230% and 137% for hydrophobic and hydrophilic substrates, with an increase in the NaCl concentration from 0 to 2 wt.%. The lateral and radial hydrate growth depends on the salinity of solution, which affects the hydrate morphological behaviour.

[1] Ayaj Ahamad Ansari, Randeep Ravesh, Samarshi Chakraborty, Pradipta Kumar Panigrahi and Malay Kumar Das "CO2 hydrate formation kinetics in the presence of layered double hydroxide nanofluid", Chemical Engineering Technology, Vol. 46, No. 8, 1630–1638 (2023) https://doi.org/10.1002/ceat.202200502

[2] Randeep Ravesh, Ayaj Ahamad Ansari, P. K. Panigrahi, and M. K. Das, "Effect of Surfactant Crowding on Clathrate Hydrate Growth", Journal of Dispersion Science and Technology, (2021) DOI : https://doi.org/10.1080/01932691.2021.1915157

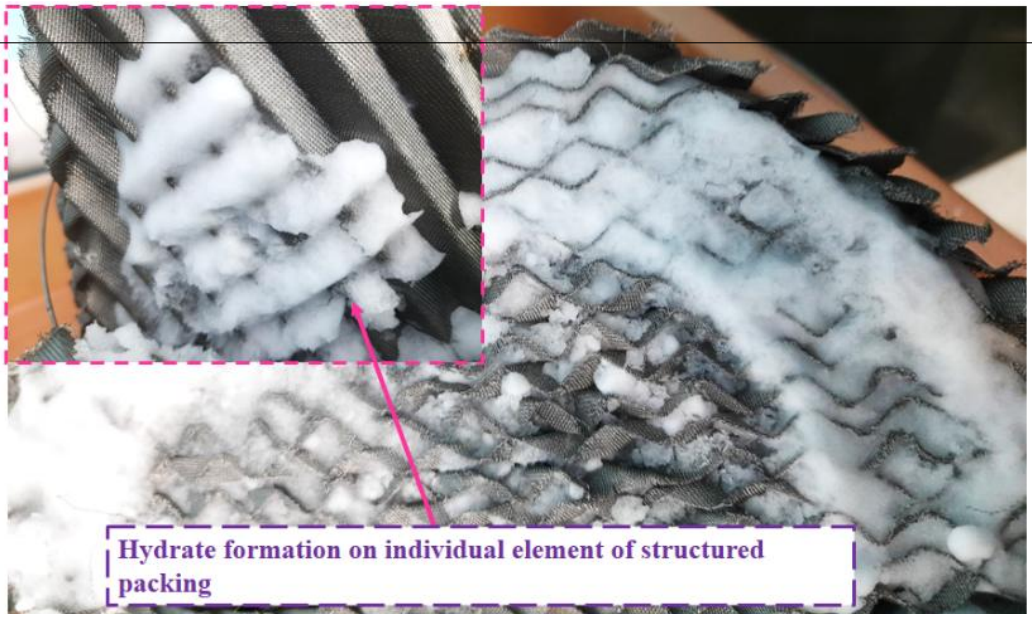

FIG. 1. Hydrate formation in a structured packing due to water migration by capillary action (Top view). The inset image shows hydrate formation across the element of packing purely due to water migration.

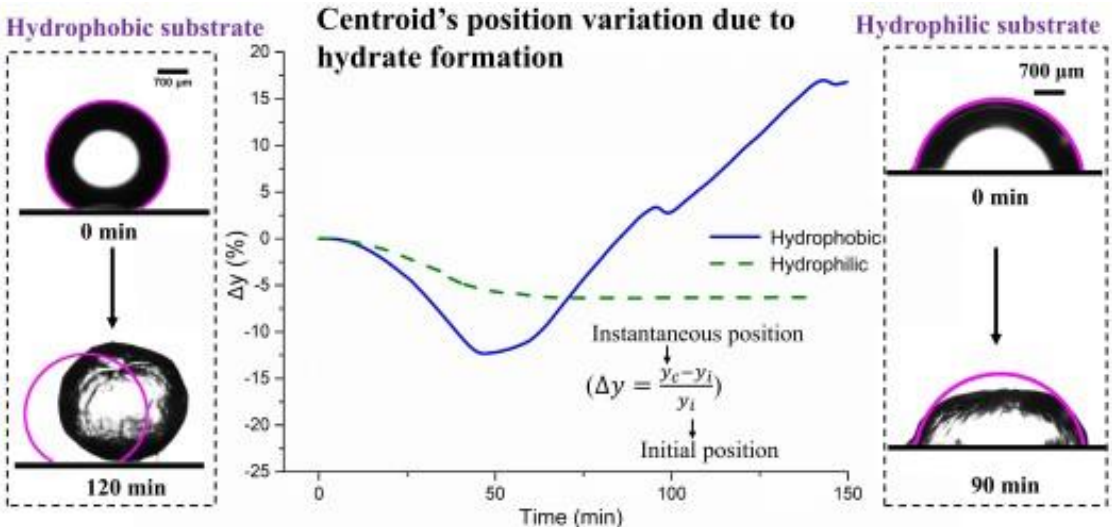

FIG. 2. The left and right side images show cyclopentane hydrate growth of a droplet on a hydrophic and hydrophobic surface respectively. The middle plot shows the evolution of droplet centroid location for hydrophilic and hydrophobic substrate.

Mass and Momentum Transfer at fluid-porousinterfaces: Jump Boundary conditions for non-parallel Flows

Christian Ruyer-Quil[1] , Sanghashri Mukhopadhyay[2] and R. Usha[3]

[1] *LOCIE UMR5271 Université Savoie Mont Blanc , 73000, Chambéry, France* ruyerquc@univ-smb.fr

[2] *Centre for Applied Sciences(CAS), International Institute of Information Technology Bangalore (IIITB), Bengaluru, 560100 Karnataka, India* Sanghasri.M@iiitb.ac.in

[3] *Department of Mathematics, IIT Madras, Chennai, 600036 Tamil Nadu, India.* usha234@gmail.com

Biological tissues are generally permeable and most biological processes involve permeable membranes and substrates. An example is the intestinal tract, which controls the absorption of nutrients in the human body. It is thus important to understand how a fluid and a permeable regions interact at their boundary. In this work, we limit ourselves to consider the mass and momentum transfer at the interface of a homogeneous and isotropic porous medium and an overlying fluid layer by solving a macroscopic closure problem based on the asymptotic solution to the generalized, transport equations (GTE) in the interfacial region. We obtained jump boundary conditions at the effective sharp surface dividing the homogeneous fluid and porous layers for either the Darcy or the Darcy-Brinkman equations. We discuss the choice of the location of the dividing surface and propose choices which reduce the distance with the GTE solutions. We propose an ad-hoc expression of the permeability distribution within the interfacial region which enables to preserve the invariance of the fluid-side averaged velocity profile with respect to the radius r0 of the averaging volume. Solutions to the GTE, equipped with the proposed permeability distribution, compare favorably to the averaged solutions to the pore-scale simulations (PSS) when the interfacial thickness δ is adjusted to r0 . Numerical tests for parallel and non-parallel flows using the obtained jump boundary conditions or the generalized transport equations show quantitative agreement with the GTE solutions, with experiments and pore-scale simulations. The proposed model of mass and momentum transport is predictive, requiring solely information on the bulk porosity and permeability and the location of the solid matrix of the porous medium. Our results suggest that the Brinkman corrections may be avoided if the ratio a = δ /δB of the thickness δ of the interfacial region to the Brinkman penetration depth δB is large enough, as the Brinkman sub-layer is entirely contained within the interfacial region in that case. Our formulation has been extended to anistropic porous media and can be easily dealt with for three-dimensional configurations.

Phase-field modeling for bubble rise near the liquid-vapor critical point

Deewakar Sharma, Arnaud Erriguible** & Sakir Amiroudine*

*Univ. Bordeaux, CNRS, Bordeaux INP, I2M, UMR 5295, F-33400, Talence, France
**Univ. Bordeaux, CNRS, Bordeaux INP, ICMCB, UMR 5026, F-33600 Pessac, France.

Recent technological advancements addressing some of the key global challenges such as, efficient energy processes for climate change, search for alternate fuels etc., have pushed the operating conditions in processes to high pressure and/or temperature conditions. The fluid in these systems is thus subjected to thermodynamic conditions which are close to the liquid-vapor critical point (termed as critical point henceforth) and sometimes move across it exhibiting phase transitions. The peculiarity of the critical point lies in the behavior of various thermophysical properties showing singularity at the critical point [1]. One such unusual behavior is the high isothermal compressibility of the liquid phase which becomes comparable to that of vapor phase when approaching the critical point. For understanding the complex fluid dynamics near the liquid vapor critical point, the first step lies in understanding the two-phase flow with both phases being highly compressible yet being in subsonic regime in isothermal conditions. This necessitates developing an appropriate model which can account for compressibility of both the phases. In this work, we address this gap in the literature by proposing a two-phase model based on phase-field modeling and extend it to study the canonical problem of vapor bubble rising in the liquid phase.

The phase-field model proposed in this work is based on using a scalar phase field parameter ϕ denoting mass fraction of phase 2 to distinguish between the two phases. The advantage of this approach is the feasibility to define the interface thickness which is computationally realistic. As the proposed model is flexible in terms of accounting for compressibility of both the phases independently, it can be used for a wide range of two-phase systems, i.e. incompressible-incompressible, compressible-incompressible. We validate the model with various canonical cases – rise of lighter fluid bubble in a heavier fluid for density ratio of 10 and 1000 and present a comparison with the experimental studies for the rise of oxygen bubbles in the liquid oxygen at the thermodynamic conditions where the compressibility of both phases cannot be neglected.

Governing equations

The phase field model considered in the present work uses mass fraction as the order parameter (ϕ) as described in [2] in conjunction with the compressible model as described in [3, 4]. The governing momentum equation for compressible fluid in terms of the scalar variable (ϕ) can be written as [2],

$$\frac{d\boldsymbol{V}}{dt} = -\boldsymbol{\nabla}P + \boldsymbol{\nabla}(\rho\bar{\alpha}|\phi|^2 - \rho\bar{\alpha}\,(\boldsymbol{\nabla}\phi \otimes \boldsymbol{\nabla}\phi)\,) + \boldsymbol{\nabla}\cdot(\mu\boldsymbol{\nabla}\boldsymbol{V}) + \boldsymbol{\nabla}\big((\lambda + \mu)\,\boldsymbol{\nabla}\cdot\boldsymbol{V}\big) \tag{1}$$

The total free energy of the system is given by, $\rho\bar{\beta}f_0(\phi) + \rho\frac{\bar{\alpha}}{2}|\boldsymbol{\nabla}\phi|^2$, here $\bar{\alpha}$ and $\bar{\beta}$ are related to the surface tension and the interface thickness. Further, $f_o(\phi) = \phi^2(1-\phi)^2$ defines the classical double-well potential form of the bulk free energy. For a compressible isothermal system, the equation of state defining the relation between pressure, order parameter ϕ, and density and can be described by $P = P(\rho, \phi)$. We can therefore write for small variations in P with ϕ and ρ with time as,

$$\frac{dP}{dt} = -\frac{1}{\chi_T}\boldsymbol{\nabla}.\boldsymbol{V} + \left(\frac{\partial P}{\partial \phi}\right)_{T,P}\frac{d\phi}{dt} \tag{2}$$

Here, χ_T is the isothermal compressibility. Further, from thermodynamics, we know $P = \rho^2\left(\frac{\partial f_b}{\partial \rho}\right)$ where $f_b = \rho\bar{\beta}f_0$ denoting the total bulk free energy. By integration of Eq. (2) over a small timestep δt, we get $P = P^0 - \boldsymbol{\nabla}.\boldsymbol{V}\delta t\ \frac{1}{\chi_T} + Y\delta t$, with $Y\ = \rho\bar{\beta}f_o'\,\boldsymbol{\nabla}.(M\boldsymbol{\nabla}\eta\,)$, $\eta = \frac{\delta F_V}{\delta \phi}$ is the chemical potential, M is the mobility parameter and P^0 is the reference pressure. Substituting this expression of pressure in Eq. (1) and using Stokes relation we get,

$$\rho\frac{d\boldsymbol{V}}{dt} = -\boldsymbol{\nabla}\left(P^0 - \boldsymbol{\nabla}.\boldsymbol{V}\frac{\delta t}{\chi_T} + Y\delta t\right) + \boldsymbol{\nabla}(\rho\bar{\alpha}|\phi|^2 - \rho\bar{\alpha}\,(\boldsymbol{\nabla}\phi \otimes \boldsymbol{\nabla}\phi)\,) + \boldsymbol{\nabla}\cdot \left(\mu\left(\boldsymbol{\nabla}\boldsymbol{V} + \boldsymbol{\nabla}^t\boldsymbol{V} - \frac{2}{3}\boldsymbol{\nabla}\cdot\boldsymbol{V}\,\underline{\underline{I}}\right)\right) \tag{3}$$

This momentum equation is solved with continuity equation to obtain density field while pressure is

calculated using the expression presented above. The phase-field variable (ϕ) is evaluated from Cahn-Hilliard equation in order to complete the model and can be written as,

$$\frac{\partial \phi}{\partial t} + \boldsymbol{V}.\nabla\phi = \frac{1}{\rho}\nabla.(M\nabla\eta) \tag{4}$$

The mobility parameter M is evaluated based on adaptive thickness approach as described in [5].

Results

We present results for two cases: (i) the rise of a lighter incompressible fluid in heavier incompressible medium with density ratio 10 in order to test our model, and (ii) a comparison with experimental data for the rise of a vapor oxygen bubble in its liquid which is also compressible [6]. In the former case, incompressibility of both the phases is accounted by setting their compressibility very small ($\chi_T = 10^{-14}\ Pa^{-1}$) rendering their behavior incompressible to the numerical precision. Figure 1 shows the results obtained with the current model for the two cases. The comparison for the rise of the oxygen bubble in its compressible liquid state at 90.1 K, atmospheric pressure of 1 bar, and the influence of the gravity field of $0.4g$ as described in [6] shows a good agreement thereby validating our model.

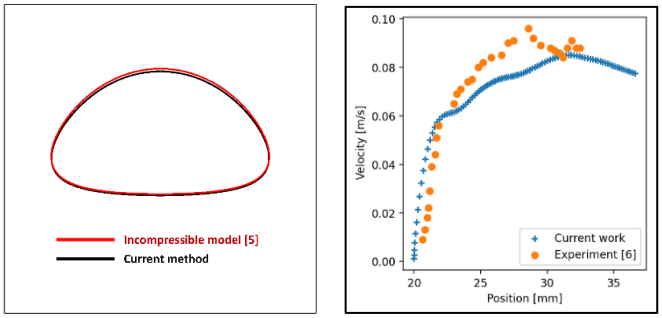

Fig. 1: Test cases comparing the bubble rise dynamics for: (from left to right)- density ratio 10 at $t = 3$s | Comparison with experimental work for rise of oxygen bubble in liquid oxygen at 90.1K where compressibility of liquid phase is ~ 10 times than that of water.

Conclusion

The presented work highlights a new model which permits to account for fluid compressibility of each phase separately and has been validated with experimental data issued from the literature. This model will be applied to the problem of vapor bubble rise in its liquid state near the liquid-vapor critical point where compressibility of both the states becomes comparable.

III. REFERENCES

[1] B. Zappoli, D. Beysens, Y. Garrabos, Heat Transfers and Related Effects in Supercritical Fluids, 1st ed., Springer Netherlands, 2014. https://doi.org/10.1007/978-94-017-9187-8.
[2] Z. Guo, P. Lin, A thermodynamically consistent phase-field model for two-phase flows with thermocapillary effects, J. Fluid Mech. 766 (2015) 226–271. https://doi.org/10.1017/jfm.2014.696.
[3] S. Amiroudine, J.P. Caltagirone, A. Erriguible, A Lagrangian–Eulerian compressible model for the trans-critical path of near-critical fluids, Int. J. Multiph. Flow 59 (2AD) 15–23. https://doi.org/10.1016/j.ijmultiphaseflow.2013.10.008.
[4] D. Sharma, A. Erriguible, S. Amiroudine, Numerical modeling of the impact pressure in a compressible liquid medium: application to the slap phase of the locomotion of a basilisk lizard, Theor. Comput. Fluid Dyn. 31 (2017) 281–293. https://doi.org/10.1007/s00162-017-0422-4.
[5] D. Sharma, M. Coquerelle, A. Erriguible, S. Amiroudine, Adaptive interface thickness-based mobility-Phase-field method for incompressible fluids, Int. J. Multiph. Flow 142 (2021) 103687. https://doi.org/10.1016/j.ijmultiphaseflow.2021.103687.

Decay dynamics of a single spherical domain close to a near-critical interface in phase-separated conditions

Raphael Saiseau,[1,2], Henri Truong,[1,3] Thomas Guérin,[1] Ulysse Delabre,[1] and Jean-Pierre Delville[1,*]

[1] *Univ. Bordeaux, CNRS, LOMA, UMR 5798, F-33400, Talence, France.*
[*] *jean-pierre.delville@u-bordeaux.fr*
[2] *Department of Physics, University of Konstanz, Konstanz 78457, Germany*
[3] *Univ. Bordeaux, CNRS, CRPP, UMR 5031, F-33600, Pessac, France.*

Domain decay is at the heart of the so-called evaporation-condensation Ostwald-ripening regime of phase ordering kinetics in conserved systems [1]. In this regime, the growth of large domains occurs at the expense of smaller ones, which are expected to 'evaporate', due to the increase of the critical radius toward completion, as nicely demonstrated by the classical evaporation-condensation LSW theory of Lifshitz, Slyozov [2] and Wagner [3]. The decay of the smallest domains was clearly observed in two dimensional systems, such as metallic islands [4] or during a liquid-solid transition triggered in confined geometry [5] in order to illustrate the importance of correlations between evolving domains. In three dimensions, its investigation was essentially indirect as most coarsening experiments, performed at the scale of a large number of interacting droplets, and measured by scattering techniques [6] or by direct visualization of droplet assemblies [7], focus instead on the evolution of the droplet distribution and its comparison to LSW predictions. So, although at the basis of the evaporation-condensation Oswald-ripening, the surface-tension driven evaporation of small droplets in conserved order parameter systems remained almost unexplored at the level of the droplets.

Starting from a near-critical phase-separated liquid mixture at equilibrium, to keep the universality of Ising models, we use the optical radiation pressure of a laser wave to destabilize the meniscus separating the two phases in equilibrium and induce a liquid jet of one phase into the other. Then, the laser is turned off to trigger a Rayleigh-Plateau instability [8] and jet breakup into droplets, and turn on again at lower beam intensity, to force the induced droplets to coalesce into a single one which is further pushed opto-mechanically to a chosen altitude, see Figure 1. Thermodynamically out-of-equilibrium due to its finite size, the produced droplet immediately starts to evaporate while buoyancy makes it rise toward the meniscus.

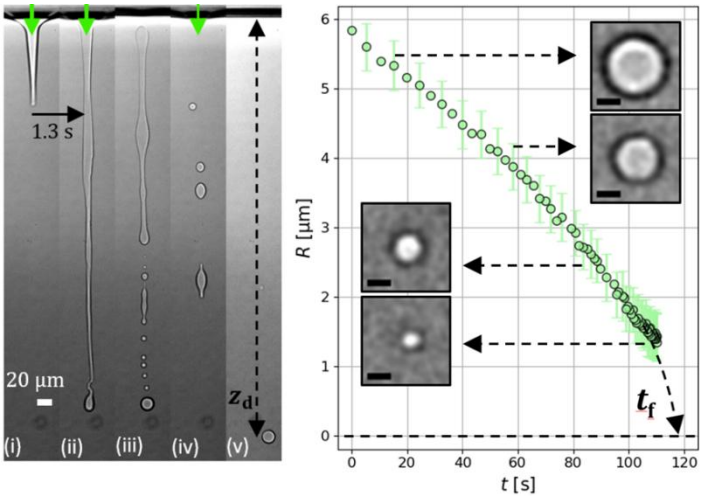

Figure 1: Left. Typical image sequence for droplet formation. (i, ii) interface instability and jet formation, (iii) Rayleigh-Plateau instability when turning off the laser, (iv) radiation pressure effect at lower laser power to force droplet coalescence, and (v) resulting final evaporating droplet optically pushed to a given altitude. Right. Droplet decay dynamics for $\Delta T = 4$ K, when the laser is permanently turned off. Scale bars : 5 µm.

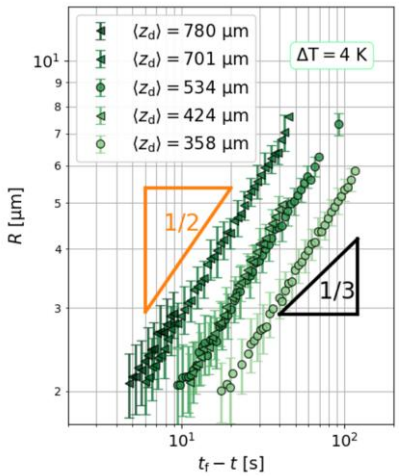

Figure 2. Droplet radius R as a function of $(t_f\text{-}t)$ for $\Delta T = 4$ K. $R\sim(t_f\text{-}t)^{1/3}$ is expected in the absence of gravity effect, which is at variance with measurements: $R\sim(t_f\text{-}t)^{1/2}$. t_f is the final evaporation time.

Figure 2 shows that the decay dynamics is generally not compatible with the theoretically

expected surface-tension decay laws for conserved order parameters (gravity-free: $R\sim(t_f-t)^{1/3}$, t_f is the final evaporation time). Using a mean-field description, we quantitatively explained this apparent discrepancy by a mechanism of barodiffusion, i.e. the presence the gradient of solute concentrations induced by gravity close to a critical point, which accelerates the dynamics of evaporation ($R\sim(t_f-t)^{1/2}$). Finally, we determined the conditions for which buoyancy becomes negligible compared to capillarity and perform dedicated experiments that retrieve the predicted surface-tension induced decay exponent. The surface-tension driven decay dynamics of conserved order parameter systems in the presence and the absence of gravity [9], is thus established at the level of a single domain.

References

[1] Bray, A. J. (1994). Theory of phase-ordering kinetics. Advances in Physics, 43(3), 357-459.

[2] Lifshitz, I. M., & Slyozov, V. V. (1961). The kinetics of precipitation from supersaturated solid solutions. Journal of physics and chemistry of solids, 19(1-2), 35-50.

[3] Wagner, C. (1961). Ostwald ripening theory. Ber. Bunsenges. Phys. Chem, 65, 581-591.

[4] Morgenstern, K., Lægsgaard, E., & Besenbacher, F. (2001, November). Decay of two-dimensional islands on Ag (110). In Collective Diffusion on Surfaces: Correlation Effects and Adatom Interactions: Proceedings of the NATO Advanced Research Workshop on Collective Diffusion on Surfaces: Correlation Effects and Adatom Interactions Prague, Czech Republic 2–6 October 2000 (pp. 201-212). Dordrecht: Springer Netherlands.

[5] Krichevsky, O., & Stavans, J. (1995). Ostwald ripening in a two-dimensional system: Correlation effects. Physical Review E, 52(2), 1818.

[6] Cumming, A., Wiltzius, P., Bates, F. S., & Rosedale, J. H. (1992). Light-scattering experiments on phase-separation dynamics in binary fluid mixtures. Physical Review A, 45(2), 885.

[7] Alkemper, J., Snyder, V. A., Akaiwa, N., & Voorhees, P. W. (1999). Dynamics of late-stage phase separation: A test of theory. Physical review letters, 82(13), 2725.

[8] Petit, J., Rivière, D., Kellay, H., & Delville, J. P. (2012). Break-up dynamics of fluctuating liquid threads. Proceedings of the National Academy of Sciences, 109(45), 18327-18331.

[9] Saiseau, R., Truong, H., Guérin, T., Delabre, U., & Delville, J. P. (2024). Decay dynamics of a single spherical domain in near-critical phase-separated conditions. Physical Review Letters, 133(1), 018201.

Passive Interfacial Evaporation-based Solar Thermal Desalination Systems

Nabajit Deka and Susmita Dash

Department of Mechanical Engineering, Indian Institute of Science, Bangalore, India, 560012

Abstract

Passive solar-thermal desalination systems present a promising solution for freshwater generation in decentralized and off-grid settings. This talk presents advances spanning fundamental wicking phenomena to the development of a scalable and salt-resistant desalination system with high water collection efficiency. The first part of the talk focuses on the role of evaporation in capillary wicking in a porous medium. A coupled mass, momentum, and energy transport model reveals a non-monotonic dependence of wicking length on channel width in rectangular microchannels—contrasting the monotonic trends in non-evaporative systems. Experiments using water and ethanol validate the model and provide geometric design criteria for enhancing evaporation rates for phase change devices.

The second part of the talk discusses a capillary-fed interfacial solar-thermal desalination system. The multistage desalination system utilizes metallic textured substrates acting as wick and evaporator. We investigate the effects of interfacial evaporation, latent heat recycling, and condenser surface properties on water collection efficiency. Patterned wettability condenser enhances condensation and increases freshwater yield by ~21% compared to unpatterned designs. To overcome limitations such as salt accumulation and limited scalability, we introduce a siphon-driven multistage system incorporating a composite siphon made of fabric and a grooved metallic substrate. A thermodynamic model based on heat and mass transfer identifies the key design and flow parameters for enhancing the system performance. The system is scalable and operates stably even in high-salinity brine. The design considerations in the evaporator and condenser facilitate a low air gap of 2 mm without liquid bridging. This design enables one of the highest distillate fluxes (~5.73 $Lm^{-2}hr^{-1}$ under 1 sun), underscoring the potential of such systems for efficient freshwater production using solar energy or waste heat source.

Faraday Instability of an Isothermal Binary Mixture Described by a Phase Field

Michael Bestehorn[1], Rodica Borcia[1] and Deewakar Sharma[2], Sakir Amiroudine[2]
[1]*Institut für Physik, BTU, 03044, Cottbus, Germany* bestehorn@b-tu.de
[2]*I2M UMR Centre National de la Recherche Scientifique 5295, Université Bordeaux, Talence, F-33400*

We study a binary fluid mixture using a phase field description. We consider a fluid pair that is immiscible for temperatures below a critical one (consolute temperature, T_c) and miscible above T_c. We derive an extended phase field equation that allows to move from the immiscible state (governed by a Cahn-Hilliard equation) to the miscible state (ruled by a species diffusion equation), where a uniform temperature serves as control parameter.

The whole system is mechanically excited showing Faraday instability of a flat interface. A linear stability analysis is performed for the stable case (interface waves) as well as for the unstable Faraday one. For the latter, a Floquet analysis shows the well-known Arnold's tongues as a function of the consolute temperature and the depth of the layer. Moreover, 2D finite difference simulations are performed allowing to model nonlinear flow patterns both in miscible and immiscible phases, see the figure below. Linear theory and non-linear simulations show interesting results such as the diminishing of wavelength of Faraday waves or a shift of the critical vibration amplitude when the consolute temperature is approached [1].

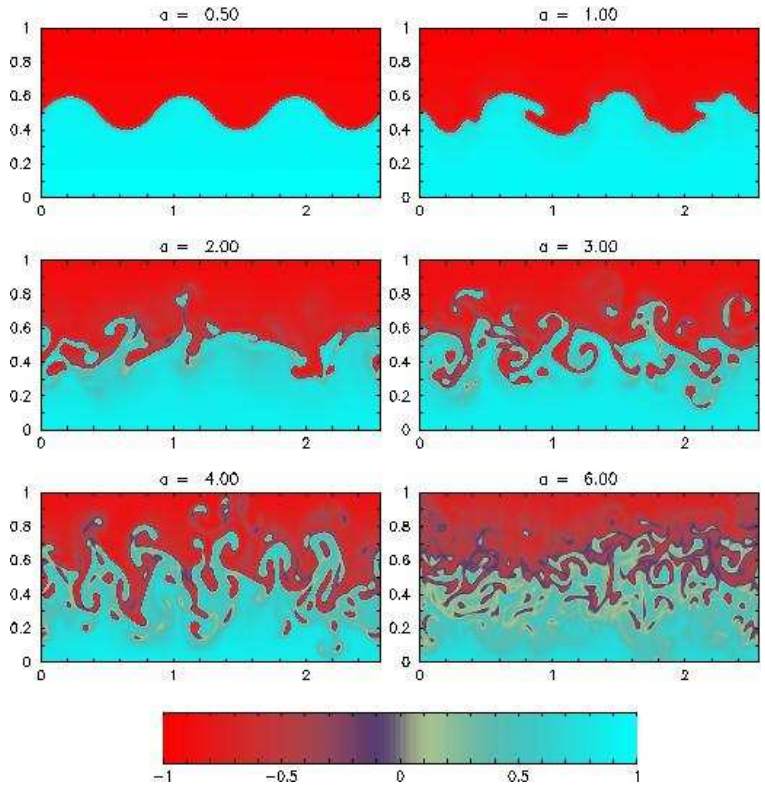

FIG. 1: Faraday instability of an immiscible fluid pair below T_c, from [1].

[1] M. Bestehorn, D. Sharma, R. Borcia and S. Amiroudine, Faraday instability of binary miscible/immiscible fluids with phase field approach, Phys. Rev. Fluids **6**, 064002 (2021).

Thwarting evaporative instability via resonance driven flows

Dinesh Bhagavatula[1], Dipin S. Pillai[2] and Georg F. Dietze [3]

[1] *Department of Chemical Engineering and Technology, IIT-BHU, 221005, Varanasi, India,* dinesh.che@iitbhu.ac.in

[2] *Department of Chemical Engineering, IIT Kanpur, 208016, Kanpur, India,* dipinsp@iitk.ac.in

[3] *Universite Paris-Saclay, CNRS, FAST, 91405, Orsay, France*, georg.dietze@universite-paris-saclay.fr

I. Abstract

In this work, we investigate the stabilization of evaporative instability through resonance-driven flows. Here we consider a hermetically sealed liquid-vapor bilayer. The liquid side wall is maintained at a higher temperature while the vapor side wall is maintained at a colder temperature. Now, if we impose a mechanical perturbation on the interface, the trough gets closer to the hot plate and the crest gets closer to the cold plate. At the trough, the perturbation then results in a stronger temperature gradient in the liquid and a weaker temperature gradient in the vapor phase. Therefore, more heat is transferred from the liquid to the interface and less heat is transferred away to the vapor phase, causing evaporation at the trough. This results in the trough getting deeper, reinforcing the perturbation and causing the interface to be unstable. Evaporative instability, often characterized by long-wave disturbances, can lead to rupture of either the liquid or vapor layer depending on system parameters, ultimately resulting in dryout and significantly impaired heat transfer performance [1].

Effective strategies to suppress the evaporative instability remain elusive. Our central focus is on prevention of a dryout and if so, what is the underlying mechanism that enables this while maintaining optimal heat flux? We propose that resonance-driven waves [2], induced by parametrically forcing the liquid in contact with its vapor, offer a viable suppression mechanism. In this context, the work of Ignatius et al. (2024) [3] is especially relevant, as they used a reduced-order long-wave model based on the Weighted Residual Integral Boundary Layer (WRIBL) approach [4] to demonstrate both linear and nonlinear suppression of Marangoni instabilities via parametric forcing. Their results in the absence of evaporation, showed that dryout could be avoided either by fully stabilizing the flat free surface or by creating a nonlinearly saturated state of standing Faraday waves at the interface. Building on this framework we consider a liquid-vapor bilayer with evaporation and without the effect of Marangoni driven flow. Here we first develop a reduced-order model using the WRIBL method which now includes the effect of resonant forcing on the evaporative instability. We then conduct a linear stability analysis to determine the critical amplitude of forcing required to either suppress the evaporative instability or initiate resonance-driven interfacial waves. These findings are further explored through nonlinear simulations that capture the dynamic evolution of the vapor-liquid interface.

[1] Pillai, D. S., & Narayanan, R. (2018). Linear and nonlinear aspects of Marangoni and evaporative instabilities. *Fluid Dynamics Research*, *50*(5), 051411.

[2] Dinesh, B., Livesay, J., Ignatius, I. B., & Narayanan, R. (2023). Pattern formation in Faraday instability—experimental validation of theoretical models. *Philosophical Transactions of the Royal Society A*, *381*(2245), 20220081.

[3] Ignatius, I. B., Dinesh, B., Dietze, G. F., & Narayanan, R. (2024). Influence of parametric forcing on Marangoni instability. *Journal of Fluid Mechanics*, *981*, A8.

[4] Kalliadasis, S., Ruyer-Quil, C., Scheid, B., & Velarde, M. G. (2011). *Falling liquid films* (Vol. 176). Springer Science & Business Media.

Modelling side wall damping in confined Faraday instability systems

S. V. Diwakar[a], Vibhor Jajoo[b], Sakir Amiroudine[b], Ranga Narayanan[c], Farzam Zoueshtiagh[d]

[a] *Engineering Mechanics Unit, JNCASR, Jakkur, Bangalore, 560064, India*

[b] *Univ. Bordeaux, I2M-TREFLE, UMR CNRS 5295,16 Avenue Pey-Berland, Pessac, 33607, France*

[c] *Department of Chemical Engineering, Univ. Florida, Gainesville, Florida, 32611, USA*

[d] *Univ. Lille, CNRS, ECLille, ISEN, Univ. Valenciennes, UMR 8520 - IEMN, F-59000 Lille, France*

*Corresponding Author E-mail: diwakar@jncasr.ac.in

ABSTRACT

The manifestation of interfacial patterns, when two fluids with dissimilar but stably stratified densities are vibrated in the direction perpendicular to their common interface, is known as the Faraday instability. The patterns vary from well-ordered structures to chaos and encompass both sub-critical as well as super-critical modes of instability. Apart from the fundamental interest in understanding pattern formation, Faraday instability finds its relevance in all space-based fluidic applications since all such systems are subjected to periodic gravitational fluctuations via g-jitter. For immiscible fluid systems, the Faraday patterns depend on factors like system size, gravity, and interfacial tension that make up the system's natural frequency. Of these parameters, the present work focuses on understanding the influence of side walls in confined systems. One may note that the theoretical analysis that usually assumes laterally unconfined walls agrees well with the experiments if the imposed parametric excitation frequency is large or the side walls are sufficiently separated. At low frequencies, however, the modes occur as discrete bands, and the wavelengths typically become comparable to the cell size. The patterns, i.e., modes seen at the onset of instability, reflect the influence of side wall geometry wherein the meniscus waves dominate. Consequently, a notable mismatch exists between experimental data and the prevalent theoretical results unless the experimentally measured damping information is somehow fed back into the model. The biggest impediment in this regard, i.e., characterizing the influence of contact line dynamics and the sloshing meniscus waves, is the lack of a simple theoretical model to represent the underlying physics. To overcome this issue, the current work proposes to use a slip-length model that allows for non-zero velocities at the side walls. The extent of the slippage is managed here by the parameter called slip length, S. Since this parameter is generally unknown a-priori, we first experimentally determine the damping rate of small perturbations in the two-layer system. Then, in the theoretical framework, we adjust the slip length to match the resulting damping to the experimentally measured value. Note that a proper approximation for the velocity profiles must be chosen to obtain a closed-form solution for the theoretical damping rate. With the slip length thus obtained from matching theoretical and experimental damping values, we reformulate the Faraday instability problem in three dimensions to estimate the critical amplitude and compare it with the experimental data.

List of participants

- Amiroudine Sakir
- Amselem Gabriel
- Audéoud Gaëlle
- Auradou Harold
- Bandyopadhyay Dipankar
- Baudoin Michael
- Bestehorn Michael
- Bhagavatula Dinesh
- Bickel Thomas
- Biswas Gautam
- Bodiguel Hugues
- Cerdin Tristan
- Chakraborty Suman
- Chandrashekar Vivaswan
- Choudhury Anjishnu
- Climent Eric
- Dasgupta Ratul
- Dash Susmita
- Delville Jean-Pierre
- Dev Narendra
- Diwakar S Venkatesan
- Dixit Harish
- Douarche Carine
- Dubey Anubhav
- Dubrulle Berengere

- Fuster Daniel
- Ghosh Debasish
- Haouche Ilies
- Hwang Gilgueng
- Ignatius Igin Benny
- Josserand Christophe
- Kamath Sanjana
- Karan Pratyaksh
- Kirar Pavan
- Kuanar Geetanjali
- Lacombe Sandrine
- Laha Sampad
- Lenz Martin
- Magnaudet Jacques
- Mahapatra Chitaranjan
- Matas Jean-Philippe
- Misbah Chaouqi
- More Sandesh
- Nicolazo-Crach Victoria
- Nikolayev Vadim
- Pain Frederic
- Pan Jieyun
- Panigrahi Pradipta
- Parveen Rukhsar
- Picardo Jason
- Ray Bahni
- Rio Emmanuelle
- Ruyer-Quil Christian
- Sahu Dinesh Kumar
- Sen Ashis
- Sharma Vandana
- T Sujith

- Tomar Gaurav
- V S Devika
- Zaleski Stéphane

Author Index